Chapter 3

The Aerodynamics of Flight

G.R. Spedding

Contents

Departments of Aerospace and Mechanical Engineering, University of Southern California, Los Angeles, CA 90089-1191, USA

Advances in Comparative and Environmental Physiology, Vol. 11

Symbols

a	vortex core radius	S_d	wing disc area
A	wake area	T	stroke period thrust
A_0	area swept by wings	$\mathbf{u}$	local velocity vector
$AR \equiv 2b/c$	aspect ratio	u, v, w	velocity components in x, y, z
b	wing semi-span	$\mathbf{u}_w$	local wing section velocity
c	wing chord	$\mathbf{u}_t$	wingtip velocity
C	closed curve	U	mean, steady velocity
C_L, C_D	lift, drag coefficient	v_2	2nd moment of virtual mass
c_l, c_d	force coeff./unit length	w_i	induced velocity
C_T	thrust coefficient	W	body weight ($= mg$)
D	drag force		
D'	drag/unit length	α	angle of attack
e	aerofoil efficiency	α_i	induced angle of attack
f	feathering parameter	α_0	body angle
$\mathbf{F}$	force vector	β	stroke plane angle
g	gravitational constant	γ	wing positional angle
$H \equiv h/b$	dimensionless height	δ	small change
$\mathbf{I}$	fluid impulse	ζ	ratio of projected wake areas
J	advance ratio	η	propulsive efficiency
k_0	arbitrary constant	θ	glide angle
k	reduced frequency, based on half chord	λ	wavelength
		μ	viscosity
$K \equiv J^{-1}$	flapping frequency parameter	ν	kinematic viscosity
l	linear length scale	ξ	vorticity
L	lift force	ρ	density
L'	lift/unit length	σ	wing shape factor
m	body mass		spatial wake correction
m_2	2nd moment of mass	σ_0	correction to momentum jet
n	frequency (Hz)	τ	downstroke ratio
P	power		temporal wake correction shear stress
$q \equiv 1/2\rho U^2$	dynamic pressure		
$Q \equiv W/S$	wing loading	ϕ	stroke amplitude
r	spanwise location	ϕ_{hf}	fore/hind-wing phase angle
	turning radius	ω	radian frequency
R	total wing length	Γ	circulation
	vortex ring radius	Γ_0	total circulation
R'	dimensionless ring radius	Θ	proportional feathering
Re	Reynolds number	Λ	dimensionless amplitude
s	wake element spacing	Φ	roll angle
	surface coordinate	Ω	reduced frequency, based on semi-span
S	surface area		

1 Introduction

1.1 Flight in Animals

It is usually estimated that there are around 10^6 extant animal species in the world, of which approximately three-quarters are insects. The Pterygota, or winged insects, comprise the vast majority of these species, and save for the orders of lice and fleas, nearly all members of this subclass have functional wings at some stage

during their life cycle. Flight has evolved quite independently in the birds (class: Aves), numbering around 8000 species, and in bats, whose 850 or so species, although less conspicuous, are the most numerous, and second most widely distributed order of the class mammalia. In terms of number of species, nonflying animals might therefore be considered unusual, and the capacity for flight seems to confer certain advantages, if measures of success include the degree of dispersal and speciation.

One of the chief benefits appears to be a reduction in the cost of purposefully moving mass from A → B, and a dimensionless cost of transport, defined as the energetic cost of moving a unit weight a unit distance, is indeed generally lower for a flying animal of any given mass, *for those animals which must support their body weight*. The favourably low cost of transport is accompanied by a high rate of energy expenditure per unit time, and there are considerable incentives to improve the efficiency of flight, when it occurs. The adaptations are physiological, structural, behavioural and developmental, as well as aerodynamic, and at once place severe constraints on the operating range of the animal, while at the same time driving the evolution of a remarkable diversity of forms. It is one of the implicit assumptions behind much of the animal flight literature that energetic, and ultimately, aerodynamic considerations have a strong effect on the structure and ecology of the individual. It will be the *only* consideration in this chapter, others in this book supplying the remaining components.

In contrast to most instances of aquatic propulsion, fluid dynamic forces in flight must also support the body weight, and the (generally) nonlinear interaction between these two requirements of lift and thrust generation leads to certain interesting complications in the analysis. In common with the previous chapter, the absence of continuous rotating mechanical devices has resulted in the development of sophisticated reciprocal oscillating systems. The consequences of the periodic accelerations of the beating wings are profound; large inertial forces, significant unsteady effects and gross departures from standard linearised models may result. The degree of this departure, as measured by the relative frequency and amplitude of the beating motion, forms the basis of organisation of the chapter.

1.2 Omissions

The discussion will be focussed on animals that are capable of sustained flapping flight and weight support. The aerodynamic requirements place considerable demands on the mechanics, physiology and behaviour, and the responses of actively flying animals to these pressures allows some kind of unified treatment of the adaptations. Flying squirrels, lizards, frogs, snakes and fish could be considered as low aspect ratio gliders, but will not be specifically mentioned. The evolution of flight will not be covered, and papers by Caple et al. (1983), Rayner (1985a, 1986), Norberg (1985) and Pennycuick (1986, 1988) should be consulted for introductions to the vigorous bird and bat flight evolution debate. The usual, but somewhat arbitrary cutoff is also applied so that human-powered and human-designed flight systems are ignored. Since this book specifically concerns animal

mechanics, the fluid dynamics of plants and inanimate objects in the environment are excluded. Fortunately, there are several fascinating books which deal with such topics, for example, those by Hertel (1966), Vogel (1981), Lugt (1983), and Ward-Smith (1984). A number of excellent reviews of various aspects of animal flight have been published in recent years. The papers in Ellington (1984, I–VI) are the current point of reference for research in insect flight aerodynamics. Pennycuick (1989a) provides clear explanations and advice on many practical issues in bird flight analysis. Aspects and applications of mechanical models of bird and bat flight have been reviewed by Rayner (1986, 1988) and Norberg and Rayner (1987), and a thorough account ranging from theoretical to ecological studies of vertebrate flight has been published by Norberg (1990).

1.3 The Modelling Enterprise

It is one of the theses of this chapter that a nontrivial understanding of animal flight must be based on some kind of aerodynamical model. Ultimately, such a model must itself be based on the known physics of the flow, which, for our purposes, reduces to the application of Newton's laws to an incompressible, homogeneous fluid. Specification of the initial and boundary conditions is, in principle, sufficient for the determination of the velocity and the pressure everywhere in the flow, by direct solution of the Navier–Stokes (NS) equations. However, even if we disregard the enormous problems in achieving adequate spatial and temporal resolution, the results of such an effort may not be particularly useful because it would not necessarily be obvious how they would generalise to other conditions, and the physical processes most responsible for some observed phenomenon in the flow field would still not be evident. We would only know that the NS equations produced it, but we already knew that since that is the system we programmed in the first place, and no physical insight has been gained. An essential part of the scientific endeavour involves the deliberate abstraction of some subset of the full physical system and the construction of a model based upon the judicious selection of appropriate simplifications. A useful model makes testable predictions, the success *or* failure of which provides new information concerning the initial assumptions. Parametric tests allow the relative significance of the model components to be assessed, and refinements in the model are derived from better physical approximations.

2 Some Nondimensional Numbers

2.1 Lift and Drag Coefficients

Regardless of the complexity of the flow or of the surface over which it is moving, there only two basic mechanisms by which a force may be communicated to a body moving through a homogeneous fluid. They are: (1) the *pressure*, $p(s)$, and

(2) the *shear stress* distribution, $\tau(s)$, over the surface. By convention, the resultant force, **F**, integrated over the whole surface, is decomposed into two orthogonal components, $L \equiv$ Lift, the component of **F** normal to the freestream velocity, U, and $D \equiv$ Drag, the component of **F** parallel to U. The dimensionless coefficients of lift and drag are then

$$C_L \equiv \frac{L}{q_\infty S}, \quad \text{and,} \quad C_D \equiv \frac{D}{q_\infty S}, \tag{1}$$

where q_∞ is the dynamic pressure and S is the surface area. The equivalent sectional lift and drag coefficients are the normalised forces per unit span, at a given chord, c:

$$c_l \equiv \frac{L'}{q_\infty c}, \quad \text{and,} \quad c_d \equiv \frac{D'}{q_\infty c}. \tag{2}$$

The total drag force is the sum of the contributions from the normal pressure and tangential stresses,

$$D = D_n + D_\tau. \tag{3}$$

D_n is known also as the form drag. When there is a mean lift on the body, it is conventional to express the sum of D_n and D_τ, minus the lift-induced drag, as the profile drag, D_{pro}. This decomposition of **F** is quite simple in conventional aeronautical applications involving steady motion in a uniform flow, but is less straightforward, and not necessarily particularly helpful, when the direction and magnitude of the fluid velocities at the surface vary greatly in space or time.

2.2 Reynolds Number

The Reynolds number, $Re \equiv Ul/\nu$, is the *only* dimensionless parameter required for specification of the dynamics of incompressible flow fields with uniform density, *for a given set of boundary and initial conditions. Re* emerges directly from the NS equations governing the motion of a fluid, when the pressure, inertial and viscous terms are in equilibrium. The triply-infinite number of possible solutions where U, l, μ and ρ ($\nu = \mu/\rho$) are chosen such that Re is unchanged, are said to be dynamically similar, determined by the ratio of the inertial and viscous terms. A dimensionless drag coefficient, as defined above, will be equal for geometrically similar bodies at the same value of Re. The chord Reynolds number, Re_c ranges from $\approx 10^1$ for the smallest insects considered here, to $\approx 10^6$ for the larger birds, a difference of 5 orders of magnitude. Certain aspects of the fluid mechanics can be expected to vary considerably across this range.

2.3 Reduced Frequency

While dynamical similarity under similar boundary and initial conditions may be assured for different flows when Re is of the same order, other dimensionless

parameters enter the problem when specification of the boundary and initial conditions involves a third parameter, in addition to U and l, such as a frequency, for example. It will prove convenient to define reduced frequencies based on the mean half-chord, $c/2$, and on the semi-span, b, as:

$$k \equiv \frac{\omega \bar{c}}{2U}, \quad \Omega \equiv \frac{\omega b}{U}. \tag{4}$$

k and Ω are related via the aspect ratio, $AR \equiv 2b/c$, by $\Omega = kAR$. The circular frequency ω is an independent kinematic parameter (it does not vary simply as a consequence of variations in the steady freestream velocity, U or the lengthscale, l) and dynamical similarity of any two flows requires that both Re and k (and when appropriate, Ω) be the same. The frequency parameter Ω is proportional to the relative magnitudes of the spanwise and streamwise components of vorticity, and is a measure of the departure from the quasi-steady limit, when $k, \Omega \to 0$.

The spanwise variation in amplitude of a wing beating at frequency n (in Hz), may be taken into account, defining the ratio K, with ϕ, the wing stroke amplitude, and r, the spanwise distance from the wing root to the point of interest, as

$$K \equiv \frac{2\phi n r}{U}. \tag{5}$$

Its inverse, $J = K^{-1}$, is the advance ratio discussed by Ellington (1984, III), when $r = R$, the wing length, and so J is the ratio of the forward flight velocity to the mean wingtip velocity. We see from Eq. (4) that $J = \pi/(\phi\Omega)$, and so for typical wingbeat amplitudes where $\phi \cong \pi/2$, $J \cong 2/\Omega$.

3 Classical Aerodynamics and the Performance of Animal Wings

3.1 *2-D* Aerofoils

The forces on an aerofoil can be discussed in terms of the vorticity and circulation of the fluid, either on the aerofoil itself, or in the wake (Fig. 1). The vorticity of a fluid element,

$$\xi = \nabla \times \mathbf{u}, \tag{6}$$

is equal to twice the local angular velocity of the fluid. There may be components of this in all space coordinates, and so it is a vector quantity. When $\xi \neq 0$, the flow is *rotational*. The circulation, Γ, is the line integral of the fluid velocity around any closed curve, C,

$$\Gamma = -\oint_C \mathbf{u} \cdot d\mathbf{x}. \tag{7}$$

An intuitive, physical interpretation of this quantity is less obvious than for ξ, but when combined with the definition of the vorticity, it may be thought of as a measure of the strength of ξ, integrated over the area enclosed by C. The *Kutta–Joukowski* theorem of lift states that the lift per unit span, L', of a body is directly proportional to the circulation:

$$L' = \rho U \Gamma. \tag{8}$$

It just remains to select a value of Γ. For a given U, there is a unique value of Γ which ensures that infinite fluid velocities are not required at the trailing edge. This condition, when the separation point occurs *exactly* at the trailing edge, is known as the *Kutta condition*, and it effectively determines the lift on the aerofoil, which, for the purposes of lift calculation, may be replaced by a point vortex having this value of Γ.

Kelvin's circulation theorem, which follows from a consideration of Eq. (7) in a homogeneous, incompressible, inviscid fluid, states that the circulation around a circuit, C, will have the same value when measured over the same fluid elements comprising C, at any time, as C is followed in the flow,

$$\frac{D\Gamma}{Dt} = 0. \tag{9}$$

Let us define a large box around an aerofoil at rest, around which Γ is initially zero (Fig. 1). As the aerofoil begins to move, accelerating to some steady finite velocity, extremely high velocity gradients, and hence ξ, are generated at the trailing edge as the flow adjusts and the separation point begins to move towards the trailing edge. While the aerofoil moves on, the vorticity will be left behind, close to where it was created. The circulation, Γ, on the aerofoil must be balanced by an equal and opposite circulation, $-\Gamma$, in the wake, according to Eq. (9). When the Kutta condition is satisfied and the aerofoil has attained a steady lift, determined by Γ_0, the flow leaves the trailing edge smoothly and no more vorticity is shed into the flow. Where it started, the shed vorticity will tend to roll up into one concentrated vortex, with circulation $\Gamma_w = -\Gamma_0$, and at all times, the total circulation, defined over the whole box, remains at zero. The lift on the aerofoil can be calculated from the vorticity in the wake according to Eqs. (6), (7) and (8). Further thought experiments along these lines show that any changes in lift on the aerofoil will necessarily be accompanied by the shedding of vorticity in the wake, and so knowledge of the strength and distribution of vortex elements in the

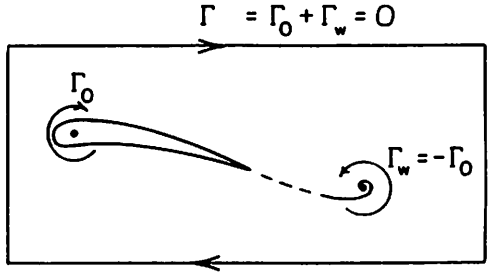

Fig. 1. The generation of bound (Γ_0) and wake (Γ_w) vorticity for an impulsively started aerofoil

wake may be used to deduce the circulation and forces on the wing. Batchelor (1967) can be consulted for an introduction to the basic fluid dynamical concepts.

Thin Aerofoil Theory. When the aerofoil thickness and camber (degree of curvature) are everywhere small, and the angle of attack, α, is small, the aerofoil can be modelled as a vortex sheet along the chord line (defined as the straight line connecting the leading and trailing edges), where the total circulation, Γ_0, is the value required to meet the Kutta condition at the trailing edge, and streamlines flow around the true cambered profile. Simple expressions may be derived for the lift coefficient and the centre of pressure showing that the centre of pressure is at the quarter chord point, and that the lift is a linear function of angle of attack. If the aerofoil is symmetric, the line of $c_l(\alpha)$ passes through the origin. Agreement with wind tunnel data for a real symmetric aerofoil is good up until a critical value of α, when the flow separates and the aerofoil stalls. When the aerofoil section shape is more complicated, the surface geometry can be defined with a number of vortex panels; the numerical solution for the circulation distribution required to satisfy the Kutta condition at the trailing edge proceeds along the same principles as before. Concise descriptions of these techniques appears in Anderson (1984), and a modern collection of aerofoil data may be found in Althaus (1980).

Reynolds Number, Flow Separation and Transition to Turbulence. Thus far, attached, high *Re* flows at small α have been implicitly assumed. In practice, for $Re < 10^6$, aerofoil performance is completely dictated by the comparatively poor resistance to separation of the laminar boundary layer. The physics of separated flows is a research topic unto itself; Lissaman's (1983) fine review contains discussion of the effects of flow separation on the performance of low *Re* aerofoils, Cheng and Smith (1982), and Cheng (1985) have reviewed and extended the theoretical analysis of laminar separation, and aspects germane to animal flight are considered by Lee and Cheng (1990). Depending on the presence or absence of flow separation and reattachment, on the location of these points on the aerofoil surface, and on the occurrence of transition to turbulence in the attached boundary layer, or in the separated free shear layer, a broad spectrum of behaviour can be observed over a critical range of $10^4 < Re < 10^6$. Two examples serve to illustrate the problem. Figure 2a shows the superior lift/drag polar of a cambered thin plate over both a flat plate, and a thin aerofoil at $Re_c = 4 \times 10^4$. Following a threefold increase in Re_c (Fig. 2b), the thin aerofoil now performs best, and with appreciably higher c_l than any of the cases at the lower Re_c. The Re_c of a bird with a mean chord of 0.1 m, gliding at $10\,m\,s^{-1}$ would be about 7×10^4. It is somewhat exasperating to note how, from the theoretical point of view, animal locomotion often appears to occur in the least convenient of all possible parameter ranges, as also noted in Chap. 2. Although laminar, attached flows can be maintained over at least portions of carefully designed aerofoils (cf. Liebeck 1978) at the top of the *Re* range above, they may be considerably disrupted by small disturbances in the flow. It is common to deliberately introduce a small perturbation at the desired transition location, so that the resulting turbulent boundary layer, by virtue of the increase in momentum

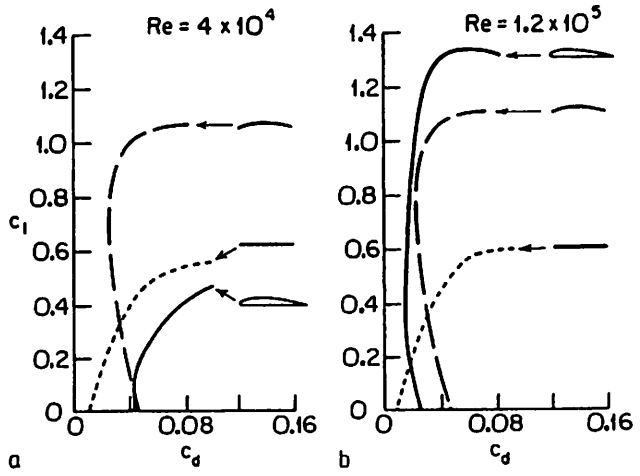

Fig. 2 a, b. Lift-drag polars for smooth aerofoils and flat plates at different Reynolds numbers. (After Jones 1990 and Schmitz 1960)

transfer from the freestream, is less unstable and more likely to withstand adverse pressure gradients along the aerofoil. Similarly, transition to turbulence in the free, separated shear layer increases the likelihood of downstream reattachment, when a *laminar separation bubble* results. For natural flight at moderate values of *Re*, turbulent flow might be the default condition, when small nonuniformities in the surface geometry (a rumpled feather) or equally small amounts of turbulence in the freestream (a gust of wind) are not unusual. Other factors influencing transition include the geometric shape of the aerofoil surface, the presence of auxiliary lifting elements, translational and rotational accelerations of the surface, and even the previous steady state of the boundary layer, as demonstrated in Fig. 3, where considerable hysteresis is observed for $c_l(\alpha)$ of a thick and thin aerofoil section at $Re_c = 10^5$. Birds and bats, operating in the $10^4 < Re < 10^6$ domain, will encounter and generate flows which are very sensitive to changes promoting or inhibiting separation and/or transition to turbulence, and the performance of their wings could fluctuate accordingly.

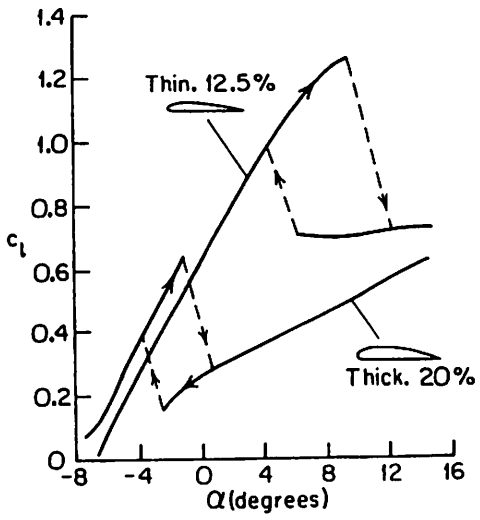

Fig. 3. Hysteresis in $c_l(\alpha)$ curves for thin and thick aerofoils at $Re = 10^5$. The formation and bursting of laminar separation bubbles is responsible for dramatic fluctuations in the lift. (After Jones 1990 and Schmitz 1960)

As Re falls below 10^3, transition is less likely, and fully laminar flow may be maintained at small α. If the laminar flow does separate, the bubble length is likely to exceed the chord length, in which case reattachment cannot occur. Due to the lack of human-scale engineering applications, available technical data on lifting surfaces at $Re < 10^3$ is quite rare, so the known behaviour of fluids at these Re in other circumstances must be cautiously applied to aerofoil and flat plate geometries. Van Dyke (1982) illustrates many fundamental low-Re fluid flows, and Lugt (1983) has discussed low Re flow over lifting bodies, including the results of some interesting numerical computations, showing how the distribution of vorticity differs in strongly separated flows at low and high Re. Intriguing flow visualisations of impulsively started *2-D* aerofoils appear also in Hertel (1966), where Re_c is probably around 10^3.

Animal Aerofoil Sections. Figure 4a shows the approximate wing sectional geometry for a bird, a bat, and two insect species, covering a range of Re_c from 10^5 to 10^2. All sections have appreciable camber, and the transition from smooth profile to flat plate with decreasing Re_c is consistent with the performance noted in Fig. 2. The pigeon section profile tapers into a very thin, extended trailing edge, bearing some resemblance to the trailing edge extensions added to low Re_c ($\approx 5 \times 10^5$), high lift aerofoils analysed by Ito (1989). The thin, tapered section is also similar in appearance to certain of the high-lift aerofoil sections reverse-engineered by Liebeck (1978), particularly when transition occurs close to the leading edge. By contrast, the bat wing membrane and supporting structures appear more like a cambered flat plate. The elastic wing membrane deforms in a passive aeroelastic response to the fluid pressures during flight, but the degree of camber may be altered by changing the tension in the membrane. In similar experiments on the gliding flight of both

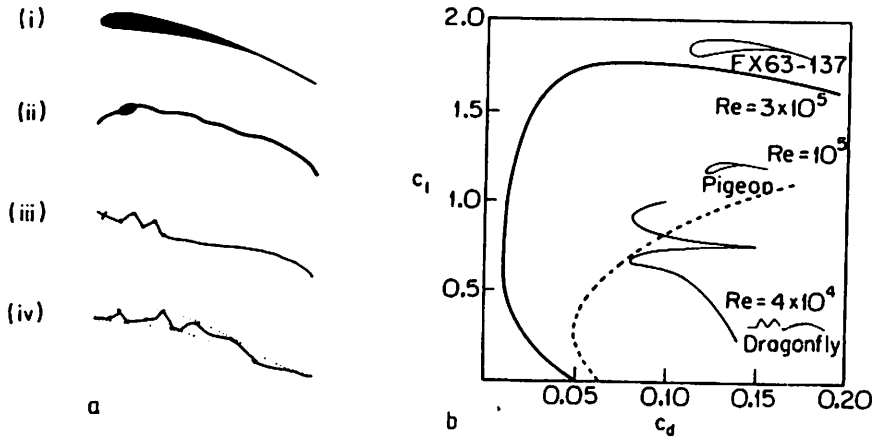

Fig. 4. **a** Wing sections of two vertebrate and two insect species, spanning a range of Re ($10^5 \geqq Re \geqq 10^2$). Based on: (*i*) Pigeon (*Columba livia*) (Nachtigall 1979). (*ii*) Dog-faced bat (*Rousettus aegyptiacus*) (Pennycuick 1973). (*iii*) Dragonfly (*Aeschna interrupta*) forewing (Newman et al. 1977). (*iv*) Hoverfly (*Syrphus balteatus*), showing smooth envelope profile used in comparison tests by Rees (1975a, b). **b** Section lift-drag polars for a modified Wortman aerofoil (Ito 1989), and models based on sections (*i*) and (*iii*)

species (Pennycuick 1968, 1971a), Re_c can be calculated as 2×10^5 for the pigeon, and 3×10^4 for the bat at the preferred gliding speeds, an interesting correspondence with the data in Fig. 2. Both insect wing sections have noticeable corrugations, which have been interpreted as promoting transition, separation and reattachment of the boundary layer for the dragonfly at $Re_c \cong 10^4$ (Hertel 1966; Newman et al. 1977). The fluid dynamics must differ somewhat at the lower $Re_c = 4.5\text{–}9 \times 10^2$ for the hoverfly profile, for which Rees (1975b) found that lift/drag polars were similar to those for an aerofoil shaped like a smooth envelope around the corrugated sheet. In this case, the primary function of the corrugations is seen as a structural adaptation for maintaining spanwise stiffness with little added wing mass inertia, and without any great aerodynamic performance reduction.

Figure 4b compares the section polars of a modified high-lift aerofoil with profiles based on sections (i) and (iii) for the pigeon and dragonfly. The performance of the pigeon section is quite respectable for the Re_c, and that of the dragonfly is rather extraordinary. Both $(L/D)_{max}$ and the slope of $c_l(c_d)$ are high, and the kink in the curve of the dragonfly section was attributed to the development of a large separation bubble entirely covering the corrugations at $\alpha \cong 8°$. The benefits of this separation bubble appear to include extended high lift regions at higher α, and the accessibility of a range of c_d at almost constant c_l. Manoeuvrable, hunting flight performance might thus be improved. Confirmation of these results would be reassuring, since Azuma and Watanabe (1988) did not find such $c_l(c_d)$ profiles in tests with miniature gliders constructed with real dragonfly hindwings.

3.2 Finite Wings

The pressure difference cannot be maintained at the tips of a finite wing, and a *rotational* motion is produced as the fluid flows around the tips. The result is thus a streamwise component of ξ, which rolls up into two trailing vortices. A vertical cut taken through the wake (Fig. 5a), illustrates the mean downward flow induced by the tip vortices. The effective angle of attack is correspondingly reduced (Fig. 5b) and the vector sum of the freestream velocity and the induced *downwash velocity* w_i, gives rise to a local velocity vector which is no longer aligned with U. Now, the local lift vector, defined as the component of the force normal to the local velocity, has a backwards component compared to the original; it adds to the total drag. This drag component is called the *induced* drag and is entirely due to the influence of the vortex-induced motion. Since these vortices were produced as a result of the pressure difference across the wing, the induced drag is an inevitable consequence of the lift. The total drag on a finite wing can now be expressed as the sum of the skin friction, pressure and induced drags [cf. Eq. (3)].

$$D = D_\tau + D_n + D_i. \tag{10}$$

D_τ is the drag due to viscous shear stress. The fact that the integrated sum of D_n over the wing surface is nonzero may also be traced to the effect of viscosity and flow separation, and the two terms are often lumped together as D_{pro}. Obviously, D_{pro} varies with Re, but it varies also with anything causing measurable changes in the

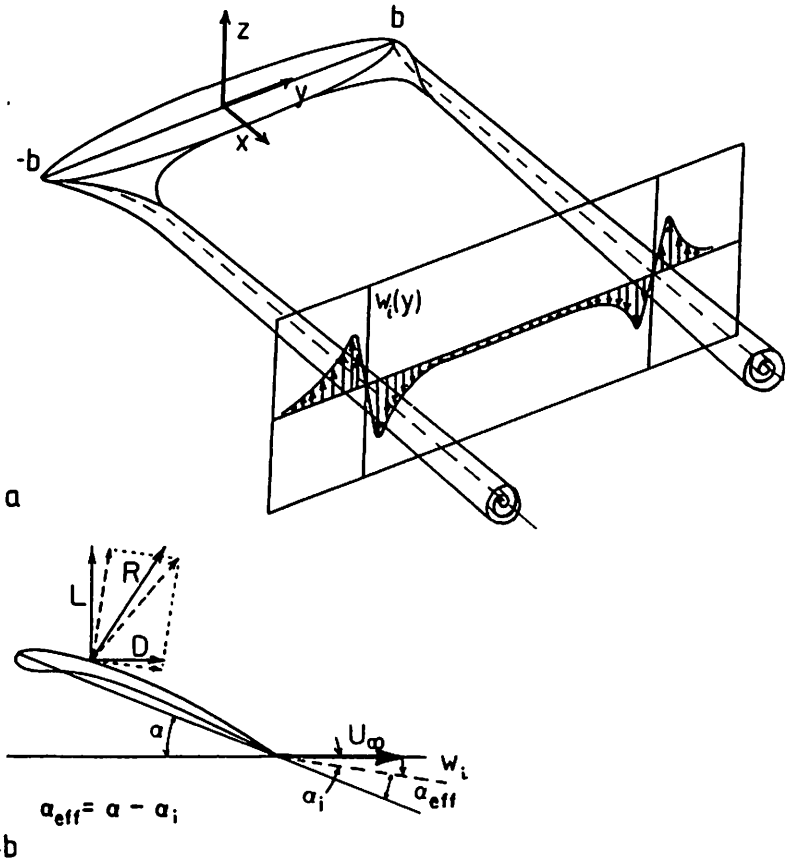

Fig. 5. **a** Wingtip trailing vortices behind a fixed wing in steady motion. y is the spanwise distance along the quarter chord line, and the total span is $2b$. The velocity profile in the vertical plane cut in the wake shows the spanwise distribution of velocity normal to the direction of motion $w_i(y)$, due to the vortex system. **b** The effect of the vertical velocity w_i is to reduce the effective angle of attack and reorient the lift vector

boundary layer flow. It is extremely hard to calculate accurately for all but the most simple flows. In practice, it is frequently estimated from empirical coefficients derived from wind tunnel tests. The remaining component, D_i, depends on the distribution of wake vorticity, which in turn depends on $\Gamma(y)$.

The Lifting Line. The action of a wing with an arbitrary, continuous $\Gamma(y)$ distribution can be analysed as a *lifting line* composed of an infinite number of coincident vortex filaments of different strengths. The wake is therefore also composed of an infinite number of line vortices and so initially has the form of a vortex sheet shed at the trailing edge. The induced drag may then be calculated, for any U, given only the form of the circulation distribution on the wing, $\Gamma(y)$. Apart from the requirement that $\Gamma(-b) = \Gamma(b) = 0$ at the wingtips, we are free, in principle, to choose any convenient $\Gamma(y)$. One possible form is an *elliptic* distribution, when an expression for C_{D_i} can easily be derived,

$$C_{D_i} = \frac{C_L^2}{e\pi AR} \tag{11}$$

where $e \leqq 1$ is the aerofoil efficiency factor. $e = 1$ when the loading is elliptic, which is therefore the optimum load distribution for minimum wake energy loss for a given lift on a planar wing in steady motion. Elliptic loading can be achieved by constructing a wing with an elliptical planform. Alternatively, the local wing section profile may vary along the span, as may the local wing twist. In practice, small deviations from elliptic loading have a rather small influence on the induced drag, and high AR, rectangular wings work tolerably well, for example. Intuitively, it seems perfectly reasonable that C_{D_i} should be proportional to the square of the lift, and inversely related to AR, since it is a physical consequence of the pressure difference at the wingtips. A more complete analysis would note that there are conflicting requirements between minimising induced drag and mean bending moments (long/short span), and between reducing both skin friction drag and maintaining sufficient structural strength (small/large chord). Jones (1990) has reviewed these requirements for fixed wings and reports that the induced drag may be reduced by about 10% over the elliptic wing, for the same integrated bending moment, by using a slightly longer wing with a more pointed tip. There is much room for further research combining both structural *and* aerodynamic considerations.

Applications of the Steady, Straight, Lifting Line. Lifting line theory provides the foundation for a large number of models in aeronautics, natural or otherwise. The numerical solution of a lifting line problem for arbitrary $\Gamma(y)$ distributions is quite straightforward, and instead of describing any particular case in detail, it is only necessary to understand the basic recipe. A wing is first divided into a number of strips at equally spaced spanwise stations, and an initial $\Gamma(y)$ is assumed. α_i is calculated at each station, y_0, and from the geometric angle of attack at that station, the effective angle of attack is given by $\alpha_{eff} = \alpha - \alpha_i$ (Fig. 5), and the section lift coefficient is determined from empirical curves for that profile; any nonlinear $c_l(\alpha)$ may thus be used. Given c_l, a new value of Γ is calculated. If it differs substantially from the old value, these steps are iterated until convergence. This algorithm is commonly used for high aspect ratio, straight wings, and derivatives of it have been widely applied to animal flight. However, *it is known to break down* whenever significant spanwise (three-dimensional) flows occur over the wing, in which case the validity of the use of *2-D* sectional lift coefficients becomes questionable.

A related technique, similar in spirit to the vortex panel analysis in *2-D*, is the lifting surface method. The wing is covered by regular arrays of vortex filaments, whose strengths vary with both x and y, which, together comprise a *lifting surface*. The induced downwash at any point on this surface is an integral of the vorticity over the lattice and the wake, and the system is solved so that the fluid velocity is everywhere tangential to the lifting surface. A variation on this theme is to cover the wing with a lattice of horseshoe vortices. The normal velocities are given by the velocity induced from all the filaments in the *vortex lattice*, and the solution proceeds as before. These are still essentially two- dimensional techniques, but the extension to *3-D* flows and geometries is relatively straightforward in principle. They are variously known as *vortex doublet* or *panel* techniques; the surface is covered with a network of vortex patches, panels or lifting lines, and at control

points on the body surface a system of linear algebraic equations is solved such that normal velocities are zero. The problem of mapping a complicated surface with an appropriate lattice mesh is often nontrivial in itself, and extremely sophisticated panelling algorithms have been developed for mapping arbitrary and/or time-varying geometries.

Animal Wing Systems. The bird, bat and insect wing planforms of Fig. 6 illustrate half of the challenge of animal flight aerodynamic analysis: how can the classical analysis be adapted and modified for application to these diverse forms? The second

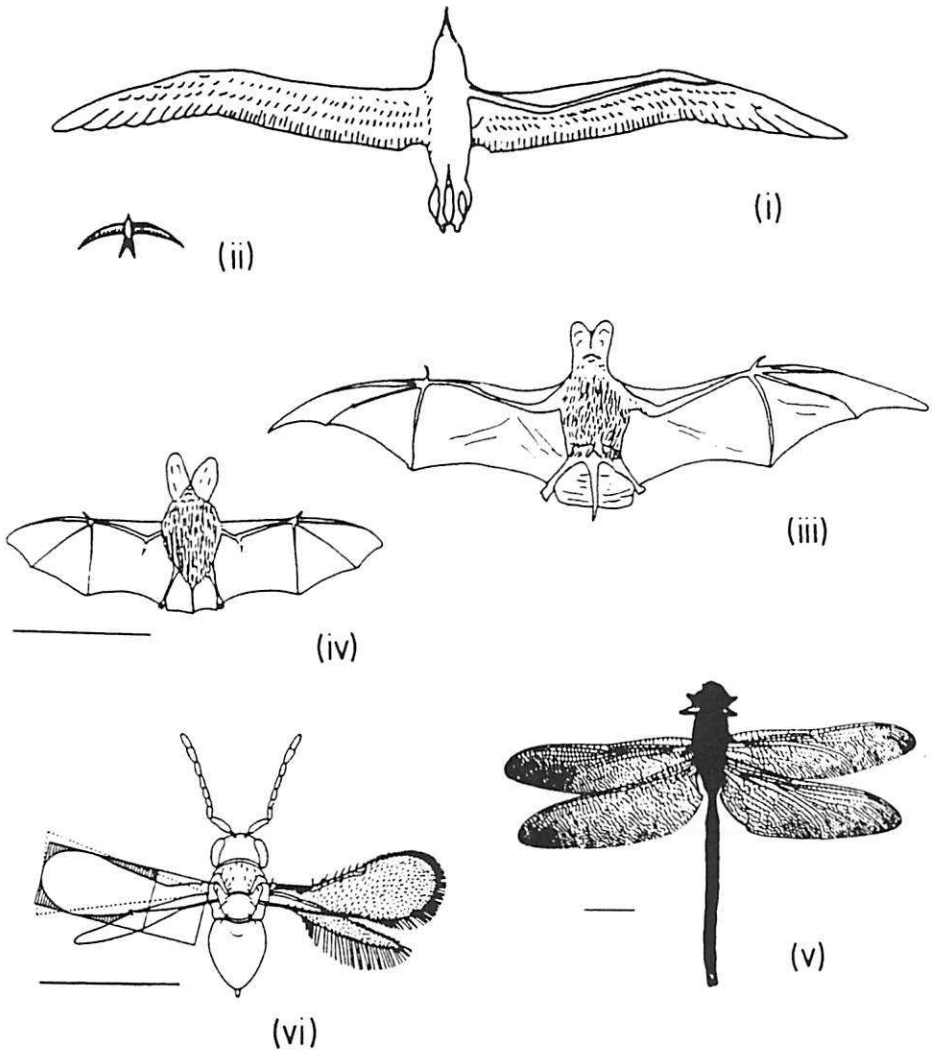

Fig. 6 (i)–(vi). The wing planforms of various birds, bats and insects. **(i)** *Diomedea* sp. and **(ii)** *Apus apus*, redrawn from Herzog (1968) to the same scale. The wing planform of *Apus* is strikingly similar to the lunate tail shape discussed in Sect. 5.5, and in Chap. 2. **(iii)** *Plecotus auritus* and **(iv)** *Otomops martiensseni*, traced from photographs in flight by U. Norberg, in Norberg and Rayner (1987) *Scale bar* 0.1 m. **(v)** *Aeschna palmata*, slightly modified from shadowgraph appearing on front cover of Somps and Luttges (1985). *Scale bar* $\approx$ 1 cm. **(vi)** *Encarsia formosa*, from Weis-Fogh (1973). *Scale bar* $\approx$ 0.5 mm. Re_c during flapping flight $\approx 1.5 \times 10^3$ and 15 for *Aeschna* and *Encarsia*, respectively. In the entire figure, the wingspan ranges from 3.4 m in the *Diomedea*, to 1.4 mm in *Encarsia*

part is to satisfactorily account for the fact that most of these wing systems experience significant oscillations for most of the time.

There have been a number of attempts to measure the planforms of animal wings in order to find general expressions for the wing shape, either to compare them with theoretical predictions, or for later use in strip-wise aerodynamic analysis. Oehme and Kitzler (1975), for example, measured the spanwise chord distribution of a number of species of birds and found that most could be approximated by a single general function, which was not an ellipse, but could be approximated by one for analytical convenience. Weis-Fogh (1973) found that many insect planforms could be approximated by a small number of simple functions, and Ellington (1984, II) has since measured the moments of mass and area for 18 insect species, with the remarkable result that the normalised wing shapes were found to lie within 5% of Beta distributions determined by one single parameter. The implication is that some strong, but as yet poorly understood, set of constraints is acting to produce such uniformity. Tantalisingly, reasonable agreement was also noted for the hummingbird *Amazilia*, and for the bat, *Plecotus*. It is likely that more is to be learned in this area.

One can also determine the wing properties empirically by measuring the $C_L(C_D)$ polar curves in wind tunnels for the complete wings, or three-dimensional models. The drag measurement therefore includes the induced drag, D_i. Figure 7 for insect wings shows that, as Re_c decreases, the maximum possible lift coefficient decreases and the sharpness of the stall decreases also. In fact, the *Drosophila* wings could hardly be said to stall at all, the drag simply continues to increase, up until

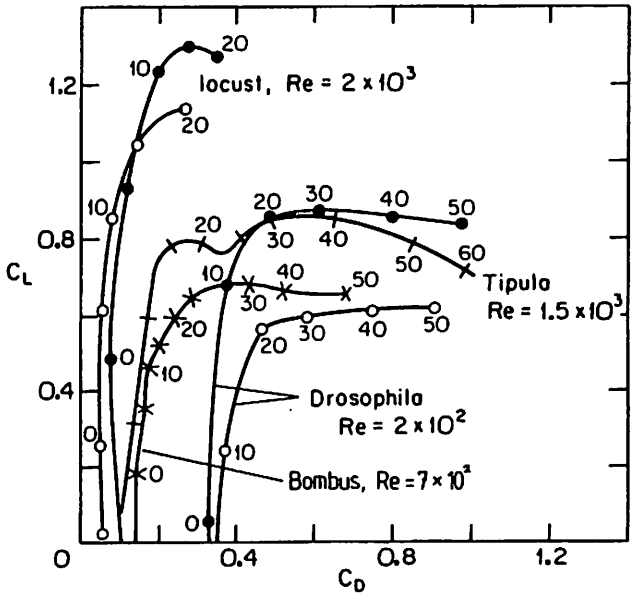

Fig. 7. Lift-drag polars for whole insect wings: Locust, *Schistocerca gregaria*, (forewing) from Jensen (1956); crane-fly, *Tipula oleracea*, from Nachtigall (1977); fruitfly, *Drosophila virilis* from Vogel (1967); bumblebee, *Bombus terrestris*, from Dudley and Ellington (1990b). *Open* and *closed circles* are for flat and cambered wings respectively

$\alpha = 50°$. At low Re_c, wings are less efficient at generating lift, but are also much less sensitive to changes in α, and will continue to function at very large α. Obtaining wind tunnel measurements of bird wings that are at all representative of the free flight performance is hampered by the complicated shape and response of the wings and feathers, and Tucker (1987) has shown that polar curves of fixed bird wings may look very different from those calculated from wind-tunnel tests on live gliding birds, due to active alteration of span and local section profiles. These difficulties would be even more acute for bat wings.

In general, animal wings are not planar, and a wing with fore or aft sweep will also be nonplanar (with respect to the freestream) when placed at some nonzero angle of attack. Cone (1962a) showed that certain nonplanar lifting systems had lower induced drag than the classical elliptically loaded planar form, and the efficiency factor e in Eq. (11) can similarly be increased, up to 1.07 behind swept wings (Burkett 1989). The large local upwash velocities associated with the sweep necessitate high values of wing twist near the tips to avoid stall there, but this effect can also be mitigated by changes in the local lifting line curvature (Cheng 1976), a geometric adaptation which does not depend on α, and which appears to have been adopted by the swift in Fig. 6(ii). Further discussion of the lunate planform in oscillating wings can be found in Chap. 2 and briefly in Sect. 5. Induced drag reduction by slotted wingtips or wingtip sails has been reviewed by Spillman (1987) and Jones (1990). The mechanism is to extract useful energy from the wingtip vortex by immersing smaller aerofoil sections in the rotating flow at the appropriate angles of attack. The cost-benefit analysis here is complicated, since the observed drag reductions could also be achieved just by increasing the aspect ratio, but it appears that induced drag reduction is effective for a wing limited in span, and for a given structural weight, when the individual winglets have variable incidence. The separated primary feathers of many bird species automatically have this property by virtue of their passive aeroelastic response to the instantaneous local airflow.

The presence of the body between the wings may be considered as another instance of nonplanarity, but the interference drag between the wings and body is probably small, and is always neglected. If there is no vortex shedding at the wing/body interface, the pressure difference across the wings is maintained across the body, whose planform area between the wings is thus included in the wing area. Otherwise, when the wing chord is small at the base, there must be considerable vortex shedding at the root, which will be reflected in the wake structure. The rest of the body is usually assumed to do no useful aerodynamic work (but cf. Csicsaky 1977), and appears instead as an extra component in the drag, the parasite drag, D_{par}.

Given these basic aerodynamic tools, and an understanding of the wings as conventional aerofoils, we are now in a position to discuss their practical operation, which we do based on three kinematic regimes of gliding, forward flight, and hovering. These correspond roughly to domains of $k = 0$, finite, nonzero k, and $k = \infty$, respectively, though it will become clear that the analytical domains do not exactly respect these boundaries.

4 Gliding

4.1 Basic Principles

Figure 8 shows the force balance on a body gliding at constant speed, U, at an angle θ with the horizontal. The lift and drag forces are

$$L = mg\cos\theta, \quad D = mg\sin\theta, \tag{12}$$

and the glide angle is determined by the ratio of lift to drag

$$\theta = \tan^{-1}\left(\frac{D}{L}\right). \tag{13}$$

The total drag on the body is the sum of the pressure and skin friction drags with the vortex-induced drag Eq. (10). From Eq. (11), the induced drag is

$$D_i = \frac{L^2}{\frac{1}{2}\rho U^2 b^2 e\pi}, \tag{14}$$

and, if the skin friction and normal pressure drags on the wings and body are combined and expressed as a profile drag coefficient (Sect. 2.1), the total drag is

$$D = \tfrac{1}{2}\rho U^2 S C_{D_{pro}} + \frac{L^2}{\frac{1}{2}\rho U^2 b^2 e\pi}. \tag{15}$$

The first term increases with U^2, while the second term, representing the energy lost in the vortex wake, decreases with U^2. At some point therefore, there will be a value of U, U_{md}, at which the total drag is minimised; if $L \approx W$ is fixed, and ignoring variations in b, S and $C_{D_{pro}}$, this point is reached when

$$U_{md} = \left(\frac{2L}{\rho b}\right)^{1/2}\left(\frac{1}{SC_{D_{pro}}e\pi}\right)^{1/4} \tag{16}$$

Lighthill (1975) noted that this defines a speed above which gliding is stable when any further increases in U will increase the magnitude of the first term in Eq. (15) which will consequently tend to reduce U. On the other hand, when $U < U_{md}$, the second term (induced drag) dominates, and increases in U will reduce the total drag, so stable gliding is not possible. As $L \sim m$, U_{md} will decrease as the mass decreases, and a simple dimensional analysis of Eq. (16) shows that $U_{md} \sim l^{1/2}$, where l is a linear dimension. Geometrically similar gliders with linear dimensions different by a factor of 10, should have characteristic gliding speeds different by

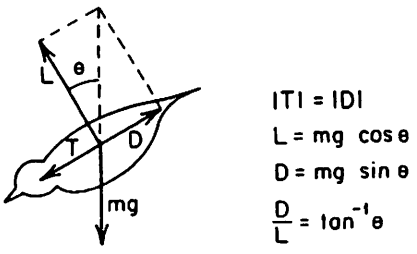

Fig. 8. The force balance on a bird gliding at constant airspeed, U, and glide angle, θ

a ratio of $10^{1/2}$, or just over 3. An alternative perspective of the minimum gliding speed may be obtained in terms of the maximum lift coefficient, since when θ is small, $L \approx mg$ [Eq. (12)], we may write

$$mg = \tfrac{1}{2}\rho U^2 S C_L, \quad \text{or} \quad \frac{mg}{S} = \tfrac{1}{2}\rho U^2 C_L. \tag{17}$$

Clearly, as U drops, C_L must increase in order to still support the weight, but C_L cannot be increased indefinitely, as flow separation occurs above a certain critical angle of attack (Sect. 3). Equation (16) shows that U_{md} may be increased either by reducing the wing area, S, or by reducing the span, b (which could also reduce S), and so animals gliding at high speed ought to reduce their wingspan, if they are able to do so. The ratio of weight to wing area, $mg/S \equiv Q$, is the *wing loading*, and is of fundamental importance in flight mechanics. According to Eq. (17), any characteristic flight speed, U^*, will be proportional to the square root of the wing loading. A low wing loading implies low gliding speeds, or, alternatively, lower freestream velocities are sufficient for continuous soaring.

4.2 Animal Gliders

The lifting line analysis is simple to apply to animal gliders, and permits testable predictions to be made concerning possible flight speeds, the geometry of the wing, and scaling laws. There is also some evidence that the lifting line assumptions behind Eq. (14) are appropriate. Quantitative flow visualisation experiments on the wake of a gliding kestrel (Spedding 1987a) showed that the wake was indeed composed of a trailing vortex pair, and calculations of Γ from velocity profiles such as that in Fig. 5 were very close to theoretical predictions. The transverse wake element spacing and the vortex core diameter were also in accordance with predicted values, and the inferred values of e and C_L were 0.96 and 1.16, respectively. This value of C_L is quite reasonable for the $Re_c \cong 4 \times 10^4$, and with $e \cong 1$ a circulation distribution close to elliptic is implied. This is consistent also with the absence of any additional concentrations of ξ in the wake caused by significant $\delta\Gamma$ on the wingspan.

The capacity to substantially vary the wing planform geometry distinguishes animal wings from many of their human-engineered counterparts, and has been observed to vary with flight speed, just as predicted in Sect. 4.1, by Pennycuick (1968, 1971a) in experiments on pigeons and bats gliding in a tilted wind-tunnel. As U increased from $8\,\mathrm{m\,s^{-1}}$ to $22\,\mathrm{m\,s^{-1}}$, the pigeon was able to reduce b to 37% of the maximum value, whilst the bat, obliged to avoid collapse of the elastic wing membrane, could reduce b to only 83% of the maximum as U ranged from 5.5 to $10\,\mathrm{m\,s^{-1}}$. The pigeon's tail feathers were unfurled at low U, providing an extra contribution to S. In terms of gliding performance, the two species were otherwise broadly comparable, with $C_{L\,max} = 1.3$ and 1.5, and $(L/D)_{\max} = 6$ and 6.8, for the bat and pigeon, respectively. Similar measurements have been made by Tucker (1987), and Tucker and Heine (1990) who reported a $C_{L_{max}}$ of 1.6 at the minimum gliding speed of a Harris' hawk.

Although both locusts and butterflies have been observed to glide frequently, their range of gliding speeds might be restricted by comparison because of their inability to substantially alter b or S during flight.

The larger gliding animals generally operate in an Re domain (10^3–10^5) where the estimation of the skin friction and normal pressure drag coefficients is highly uncertain. In the absence of flow separation, integration of the boundary layer equations gives a result for the dependence of total friction drag on Re_l as

$$D_\tau = k_0 \rho U_\infty^2 S Re_l^{-1/2}, \tag{18}$$

where Re_l is based on an appropriate streamwise lengthscale, and k_0 depends on the shape. A turbulent boundary layer grows faster than a laminar one, when Re_l enters Eq. (18) as $Re_l^{-1/5}$. These relationships have been well confirmed by experiment. The magnitude of the normal stresses on a body with a growing boundary layer depend on the boundary layer thickness, and so, all other things being equal, the normal pressure drag coefficient will also vary with $Re_l^{-1/2}$ or $Re_l^{-1/5}$. The value of D_n is in practice determined by the presence or absence of separation in the flow, and it is usually measured empirically.

The current status of measurement of D_τ and D_n on the wings and bodies of birds has been discussed by Pennycuick et al. (1988) and Tucker (1987, 1990). The observed drag coefficients on the wings and body, $C_{D_{pro}}$ and $C_{D_{par}}$, appear to decrease across the critical Re range, implying that early transition to turbulence in the boundary layer either prevents separation altogether, or moves the separation point further downstream, or assists in its subsequent reattachment. The measurements of D_{par} were extremely sensitive to the smoothness of the body surface, and drag coefficients were reduced by approximately 15% by Pennycuick et al. when the feathers were flattened with hairspray, and by 40% by Tucker when a smooth model with the same contour replaced the dead body. D_{pro} depends also on the local wing section profile and changes in b and S with flight speed, U. The relationship between any two of these parameters is not simple; in general, both C_L and $C_{D_{pro}}$ tend to *decrease* with increasing U for an intact gliding bird, but changes in wing geometry as measured by b, for example, introduce considerable variation.

It is possible that aerofoil operation around Re_{crit} plays a critical role in the gliding performance capabilities of soaring birds, but much remains to be accurately measured and understood. As a practical matter, given the tremendous uncertainties in the drag coefficient measurements, an appropriate procedure might be to first compute a value of Re_l, and then use it in a form of Eq. (18), with a suitable value of k_0 to account for experimental results when available.

4.3 Gliding Performance

Horizontal Distance Travelled. Maximising the ratio of horizontal distance travelled to vertical distance climbed is equivalent to minimising the glide angle, θ, and inspection of Eq. (13) shows that the L/D ratio is inversely related to θ. Given that $L \approx mg = W$ is a constant, then the minimum glide angle θ_{min} corresponds to gliding with the minimum possible total drag, D_{min}. The expression (16) for U_{md} thus also

defines a best glide speed, U_{bg}. Rearranging Eq. (16) slightly,

$$U_{bg} = U_{md} = \left(\frac{2W}{\rho S}\right)^{1/2} \left(\frac{1}{ARC_{D_{pro}} e\pi}\right)^{1/4}. \tag{19}$$

W has been substituted for L and U_{bg} is expressed in terms of the wing area, S, and the aspect ratio AR. The best glide speed increases with W, and decreases with both S and AR. If the objective is to extract energy from the environment and glide without loss of height, then it is useful to be capable of this for as low a value of U as possible, and there are two possibilities for minimising U_{bg}; have wings with large area, S, or have long narrow wings and increase AR. These contrasting strategies are illustrated in Fig. 9, from Pennycuick (1983), who compared the gliding performance and wing planform of the frigatebird, pelican and vulture, all of which were observed to make extensive use of thermal soaring. The frigatebird has a very low wing loading ($Q = 37\,\mathrm{Nm}^{-2}$), as well as a higher aspect ratio ($AR = 13$), compared with both the pelican and the vulture ($Q = 58$ and $55\,\mathrm{N\,m}^{-2}$, $AR = 10$ and 6, respectively), and so manages to minimise both of the terms in Eq. (19). It is distinguished by almost constant gliding and soaring in trade wind thermals for days on end, rarely coming in to land. The shorter, slotted wings of the pelican and vulture probably represent a balance between adaptations for landing and take-off and induced drag reduction for wings with limited span and low moment of inertia.

Air Time. The cross-country performance of a glider may alternatively be measured by energy consumption per unit time. In steady flight, the kinetic energy of the glider is constant, and so the rate of energy loss required to overcome drag (and generate a wake) is balanced by a reduction in potential energy, occurring at a rate mgU_s, where U_s is the vertical downward velocity, so

$$mgU_s = DU. \tag{20}$$

mg is a constant, and DU can only be minimised through U_s. The total drag was given in Eq. (15), and substituting an approximate expression of the form of Eq. (18),

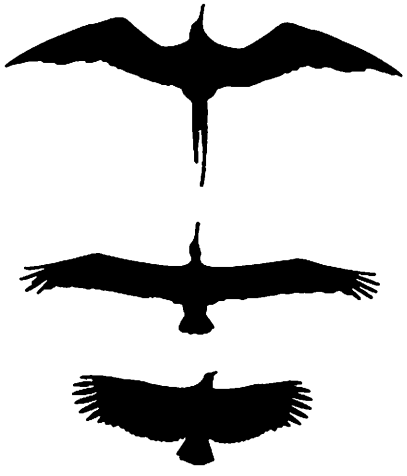

Fig. 9. Silhouettes of three gliding birds. From top: *Fregata magnificens, Pelecanus occidentalis, Coragyps atratus.* (Pennycuick 1983)

assuming a turbulent boundary layer, for the skin friction and normal pressure drag components of $D_{pro} + D_{par}$, U_s may be written in the form

$$U_s = k_0 \rho U^3 S^2 Re^{-1/5} + \frac{2W}{\rho U S A R e \pi}. \tag{21}$$

The first term in Eq. (21), due to profile drag on the wings and body, increases as S^2, while the second term from the lift-induced drag is proportional to S^{-1}, so U_s increases with S. The second term is inversely proportional to AR so a cross-country glider should have as high an aspect ratio as is structurally possible, compatible with the other flight requirements. Albatrosses have aspect ratios of around 15, while modern composites and specialised function allow $AR > 20$ in almost all man-made gliders. Equation (21) depends only on the wing geometry through S and AR, for a glider of a given weight moving with a given airspeed, U. The graph of $U_s(U)$ is called a glide polar (Fig. 10a). Because birds, and to a lesser extent bats also, have the ability to modify b and S at different U, they will occupy an envelope on this plot determined by the family of glide polars attainable from varying the wing planform. Similarly, changes in profile camber, or the recruitment of additional high lift devices, such as those discussed in Sect. 3.2, will extend the domain of available $U_s(U)$ ratios, as discussed by Tucker (1987).

Turning Radius. Glider pilots and birds (cf. Cone 1962b; Pennycuick 1975), but presumably not nocturnal bats, make extensive use of atmospheric thermals, which are most often columns of circulating and rising air, but may also be buoyant, rising vortex rings. Both are created by differential heating on the ground by solar radiation, and both are limited in horizontal extent, supplying an incentive to be able to maintain a small turning radius. In a steady, nonaccelerating turn, the centrifugal force, mU^2/r, is balanced by the component of the lift vector projected onto r, so, if Φ is the angle between the lift and the vertical,

$$\frac{mU^2}{r} = L \sin \Phi. \tag{22}$$

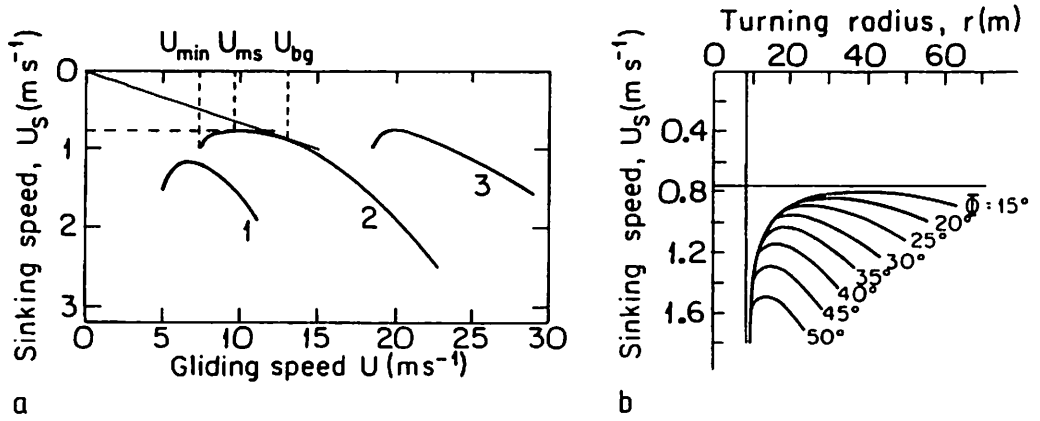

Fig. 10. **a** Glide polars for the fruit bat (*1*), *Rousettus aegyptiacus*, the white-backed vulture (*2*), *Gyps africanus*, and the ASK-14 motor glider (*3*). (Data from Pennycuick 1971a, b). **b** Family of glide polars generated for *Gyps africanus* turning at different bank angles Φ. (After Pennycuick 1975)

r is constrained by possible values of Φ and L. For convenience, one can set an upper limit for $\sin\Phi = 1$ (practically speaking, it will be much lower), and the highest value of L is determined by $C_{L_{max}}$, and so the limit on r is,

$$r_{min} = \frac{2m}{\rho S C_{L_{max}}}. \tag{23}$$

If $C_{L_{max}}$ is constant, r_{min} depends only on m/S, equivalent to the wing loading (for constant g). The component of lift opposing mg is now $L\cos\Phi$, and U_s in a turn will be related to the straight-line U_s by

$$U_{s_t} = U_s \cos\Phi. \tag{24}$$

A family of glide polars may therefore be constructed for a range of Φ (Fig. 10b). Pennycuick (1971b) examined the gliding performance of the white-backed vulture by following individuals around in a small glider, noting that these thermal soarers have comparatively low AR wings, but large wing areas. According to Eq. (23), this would appear to make them ideally suited for small radius turns, and comparisons with a hypothetical albatross-shaped vulture showed them better able to remain inside small thermals than if they had the higher AR, but lower S wing planform. However, this would be offset by the albatross-vulture's improved cross-country performance between thermals, and it seems that the difference cannot be accounted for purely in terms of aerodynamic soaring performance.

Dynamic Soaring. Lighthill (1975) outlined a surprisingly simple analysis of dynamic soaring, which we use here. Consider a body, B, in a fluid where there is a mean shear of the u component in the vertical direction, z, such as at a wall boundary layer, or over an air/sea interface. B might equally be a fluid element in a turbulent shear flow, or an albatross in a wind gradient. B has velocity

$$\mathbf{u} = \bar{u}(z) + u', v', w', \tag{25}$$

where the primed components are the fluctuating velocities in the turbulent flow, or the components of velocity of the bird, in (x, y, z). Overbars are mean quantities, and the mean shear $\bar{u}(z)$ varies only with z. The kinetic energy of B *relative to the velocity* gradient is

$$e' = \tfrac{1}{2}m(u'^2, v'^2, w'^2), \tag{26}$$

and if B is a gliding bird, e' must be maintained by performing work to overcome aerodynamic drag forces, so as to avoid stalling. The rate of exchange of total energy between B, moving at (u', v', w'), and the mean velocity gradient is

$$\dot{P} = -m\overline{u'w'}\frac{\partial \bar{u}}{\partial z}. \tag{27}$$

The magnitude of $\dot{P}$ in (27) is proportional to the magnitude of $\delta\bar{u}/\delta z$. The sign of the product $u'w'$ may be positive, implying a transfer of energy from the mean flow to the fluctuating part (the bird). This will occur when u' and w' have opposite signs; when flying into the shear, u' is negative so w' should be positive, and,

conversely, when u' is positive, w' should be negative. The required behaviour of flying upwards into wind shear, and downwards away from it has often been noted, and has been subject to quite elaborate analyses (e.g. Cone 1964; Wood 1973), but more accurate measurements of albatrosses gliding in wind shear by Pennycuick (1982) revealed that the magnitude of $\delta\bar{u}/\delta z$ would not be sufficient to maintain the kinetic energy, except very close to the water surface. Instead, there must be some conversion of kinetic into potential energy, so that the bird decelerates as it gains height, deriving most energy from slope lift in waves at the surface, much as proposed by Wilson (1975). Note that the mechanism of dynamic soaring probably still pertains, and the flight path is chosen with the sign of Eq. (27) still in mind, but that the mean shear cannot by itself supply sufficient energy. Also, the variable wing geometry that allows birds to glide at low speeds and high lift coefficients also relaxes somewhat the condition (26), more readily allowing e' to fall.

5 Forward Flapping Flight

5.1 The Principles of Lift and Thrust Generation by a Beating Wing

In the absence of any energy input from the environment, the beating wings of an animal in steady flight must provide both lift and thrust required to maintain height and forward speed. We therefore begin by outlining the kinematic basis for generating both force components from an oscillating wing section. As Lighthill (1969) noted, in order to provide weight support, some asymmetry must be introduced into the combined pitching and heaving motion of a lifting surface,

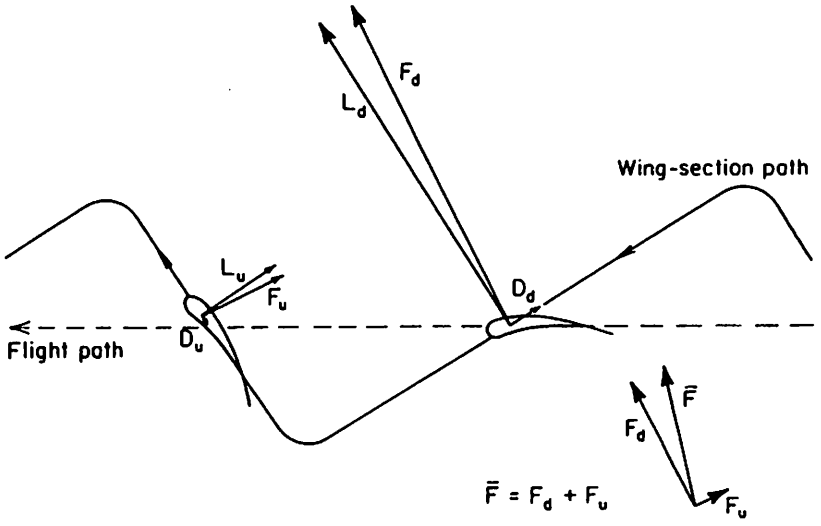

Fig. 11. The production of lift and thrust with an asymmetric wingbeat

and it is sufficient just to add a constant angle of attack to the otherwise symmetric motion of a thrust-generating wing. The easiest way to imagine doing this for a flying animal is to tilt the whole body, and/or the wings relative to the body, so that they beat in a plane inclined at an angle, β, to the horizontal. The result is analysed in Fig. 11. Owing to $\beta \neq 0$, the wings sweep forward, with respect to the wing root, on the downstroke, and backwards on the upstroke. Both the incident velocity, $\mathbf{u}$, and the geometric angle of attack, α, are larger on the downstroke than on the upstroke, and so the magnitude of the resultant force, $\mathbf{F}_d$, is greater than that produced during the upstroke, $\mathbf{F}_u$. If the time spent on up- and downstrokes is equal (the downstroke ratio, $\tau = 0.5$), and the L/D ratio is constant, Fig. 11 is a graphically accurate demonstration that the mean resultant force, $\bar{\mathbf{F}} = \mathbf{F}_d + \mathbf{F}_u$, averaged over the wingbeat, can have positive components of lift and thrust. Actually, this figure includes a second strategy for introducing the required asymmetry, as α is even further reduced during the upstroke, following a strong pitch-up rotation (or supination) at the end of the previous half-stroke. This contributes to the reduction in magnitude of $\mathbf{F}_u$. There is considerable scope for exerting fine control over the magnitude and direction of $\mathbf{F}$, via changes in α (it may even be negative), aerofoil section camber, and τ. The proportional feathering parameter, Θ, (Lighthill 1969) was introduced in Chap. 2, and it controls the local incidence angle compared to the local relative wind, effectively determining the balance between thrust and efficiency. The complicated kinematics, together with the highly variable wing geometries encountered in nature (recall Figs. 4 and 6), conspire to defeat attempts to include all possible kinematic and geometric parameters in a theoretical analysis, and the focus turns to formulating a simple model problem which can be solved, but which still captures some of the essential physics. Generally, one may proceed either by modelling the beating wing, or by constructing a simple model of the wake (recall Fig. 1).

5.2 Blade Element Analysis

The classic reference for this approach is the work of Jensen and Weis-Fogh 1956; Weis-Fogh and Jensen 1956; Weis-Fogh 1956; Jensen 1956) on the desert locust, *Schistocerca gregaria*. One of the advantages of dealing with locust wings is that their geometry and kinematics are comparatively simple, a prerequisite for this type of analysis. Figure 12a introduces the coordinate system for describing the flapping wing of an animal moving at forward speed U. The wings beat in a plane, at an angle β to the horizontal, through a total angle ϕ. The kinematic analysis starts by examining the wing position as a function of time, $\gamma(t)$. Assuming the wingbeat is sinusoidal, then

$$\gamma(t) = \bar{\gamma} + \tfrac{1}{2}\phi \sin \omega t, \tag{28}$$

where $\omega = 2\pi n$ is the radian frequency of the wingbeat. The angular velocity is

$$\dot{\gamma}(t) = \frac{\omega}{2}\phi \cos \omega t,$$

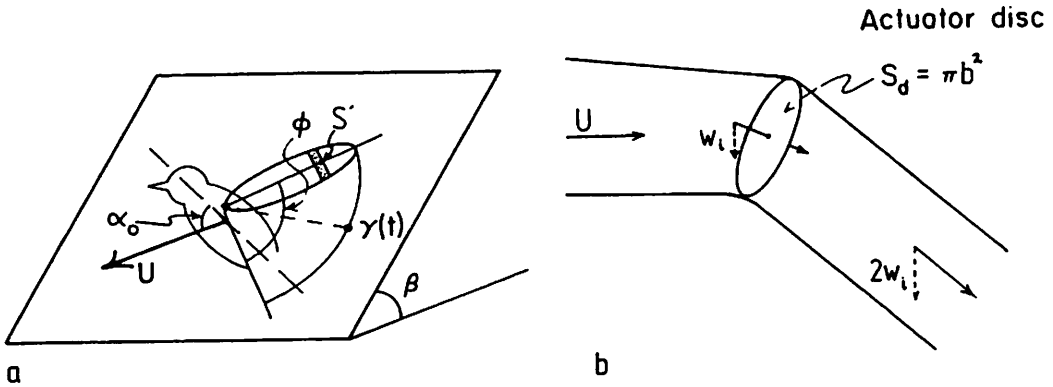

Fig. 12a, b. Two alternative perpectives for the aerodynamic analysis. **a** The kinematics of a flapping wing. **b** Wake momentum flux

so the velocity of the wing at a span section, r, and at time t is

$$\mathbf{u}_w(r,t) = r\dot{\gamma}(t) = r\frac{\omega}{2}\phi\cos\omega t. \tag{29}$$

The local incident velocity, $\mathbf{u}(r,t)$, at a wing section will depend on the resultant, $\mathbf{u}_n(r,t)$, of $\mathbf{u}_w(r,t)$, and U, the forward flight velocity, and also on $w_i(r,t)$, the downwash velocity, which alters the local angle of attack (Sect. 3.2, Fig. 5),

$$\alpha_{eff} = \alpha - \alpha_i, \tag{30}$$

where

$$\alpha_i = \tan^{-1}\left[\frac{w_i(r,t)}{\mathbf{u}_n(r,t)}\right]. \tag{31}$$

Some means of estimating $w_i(r,t)$ in (31) must be found. Commonly, it is assumed to be uniform across the span, as in the elliptically-loaded lifting line (Sect. 4.3), with a value estimated from actuator disc models (Sect. 5.3). Jensen and Weis-Fogh actually did not do this. Instead, locust wings were placed in the wall boundary layer of a wind tunnel, and the lift and drag on the entire wing in a shear flow similar to that produced by flapping about the wing root were measured. The drag thus included the induced drag, which did not have to be estimated separately.

Now, given α_{eff}, provided that all *3-D* effects can be ignored, and if steady-state aerofoil properties can be used, then c_l may be estimated from empirical $c_l(\alpha)$ data. Given $\mathbf{u}$ and c_l, the local section lift and drag forces are:

$$\left.\begin{aligned} L'(r,t) &= \tfrac{1}{2}\rho\mathbf{u}^2 c_l S' \\ D'(r,t) &= \tfrac{1}{2}\rho\mathbf{u}^2 c_d S' \end{aligned}\right\} \tag{32}$$

S' is just the wing chord, $c(r)$ at the span r, and the primes indicate that L' and D' are the components of the aerodynamic force per unit length. The mean lift is

the integral of the vertical components, L'_v and D'_v, of L' and D' over R and T,

$$\bar{L} = \frac{1}{T}\int_0^T \left\{ \int_0^R [L'_v(r,t) + D'_v(r,t)]\,dr \right\} dt. \tag{33}$$

Based on the kinematic measurements from wind tunnel flights when the locusts were measured to be supporting their weight, Jensen was then able to calculate the total lift and drag from relationships such as (32), using only three weighted averages along the wingspan. The mean lift and drag were found to agree with the measured values to within 3% and 7% for the two flights considered. Since the lift and drag coefficients had been determined in steady state wind-tunnel tests, these results were construed as convincing evidence that the aerodynamics were consistent with steady-state principles, contrary to many beliefs at the time. It was further argued that this would be *expected* to be the case, given the wingbeat kinematics and angles of attack measured during flight. The frequency parameters k, Ω and K may be calculated for a locust forewing with mean chord, $\bar{c} = 0.93$ cm, semi-span, $b = R = 5.21$ cm, forward speed, $U = 350\,\mathrm{cm\,s^{-1}}$, stroke angle, $\phi = 83°$ (1.45 rad), and wingbeat frequency, $n = 17.5$ Hz ($\omega = 110\,\mathrm{rad\,s^{-1}}$):

$$k = \frac{\omega\bar{c}}{2U} = 0.15, \quad \Omega = \frac{\omega b}{U} = 1.64, \quad K = \frac{2\phi n R}{U} = 0.755.$$

k and Ω are not exceptionally small, and the advance ratio, $J = K^{-1} = 1.32$ is relatively large, but certainly not huge. Although the authors at the time had little alternative but to proceed and use the aerodynamic forces calculated in this way to estimate the power required of the flight muscles to generate the necessary torques at the wing root, we shall later see that *3-D* and unsteady corrections can nevertheless be significant in this domain.

Further simplifications of Eq. (33) are possible. If the changes in local wing twist, sectional geometry and chord length are such as to maintain a constant value of c_l and c_d along the span, then the coefficients may simply be replaced with mean values over the whole span and wingstroke. If a constant w_i across the span is also assumed, then the problem reduces simply to finding some manageable formulation of the wingbeat kinematics and wing planform geometry. Examples of this type of approach may be found in Norberg (1976a) for bats, Pennycuick (1975) for birds, and Dudley and Ellington (1990a, b) for the bumblebee. In steady horizontal flight, the vertical components of the integrated aerodynamic forces during each wingbeat cycle must support the weight, and so one may write equations of the form:

$$\int_0^T W\,dt = \rho\bar{C}_L \int_0^T \left\{ \int_0^R \mathbf{u}^2(r,t)S'(r)\cos\psi\,dr \right\} dt + \rho\bar{C}_D \int_0^T \left\{ \int_0^R \mathbf{u}^2(r,t)S'(r)\sin\psi\,dr \right\} dt, \tag{34}$$

where the angle ψ is a much simplified representation of the required projection geometry calculations. Here it plays a role quite analogous to a projection onto the horizontal plane of the vertical impulse of the wake. This analogy should

become clearer in Sect. 5.4. A similar equation for the horizontal force projections can be written, and if $\mathbf{D}_{par}$ and $\mathbf{D}_{pro}$ can be estimated, the system may be solved for $\bar{C}_L$ and $\bar{C}_D$. The argument now shifts slightly; if reasonable values of $\bar{C}_L$ and $\bar{C}_D$ are computed, consistent with the known or likely performance of the aerofoil wings, then the initial assumptions of steady-state performance are supported. If not, some other mechanism must be significant, and unsteady effects of various kinds may be proposed. Just by itself, this is a curiously circular sort of argument, of little interest unless the numerical results are then used in subsequent calculations. The controversy over this proof by contradiction, summarised by Ellington (1984, I, IV, V), seems endless, and we shall return to it in the hovering flight discussion (Sect. 7.2). Note, however, that regardless of whether *3-D* and/or unsteady corrections are required for an accurate *aerodynamic analysis*, their relative importance in the wing aerodynamics is a slightly different issue than whether or not they *need* to be incorporated in a general flight model, and it is easy to imagine a wing which accelerates and rotates at the extremes of the wingbeat, being dominated by unsteady effects there, but overall having a performance roughly equivalent to an unspectacular mean lift coefficient averaged over the whole wingbeat. Indeed, direct measurements of the *instantaneous* lift forces on the locust-in-a-wind-tunnel experiment by Cloupeau et al. (1979) showed that the amplitudes of the fluctuations in aerodynamic lift were about two times those calculated by Jensen, while the *time-averaged* values were approximately the same, implying that unsteady effects are significant. Moreover, Dudley and Ellington's (1990b) wind tunnel experiments on the bumblebee (in free flight) for $U = 0 - 4.5\,\mathrm{m\,s^{-1}}$ indicated that the minimum required C_L values *always* exceeded 1, while the wind-tunnel tests showed the wings to be incapable of $C_L > 0.8$ in steady flow. The same frequency parameters can be calculated as for the locust, and at the top speed of $4.5\,\mathrm{m\,s^{-1}}$ one finds:

$$k = 0.40, \quad \Omega = 2.65, \quad K = 1.52.$$

The reduced frequencies are substantially higher than for the locust, and it is no longer true that $k \ll 1$. It will later be demonstrated (Sect. 5.5) that at these values of k and Ω, one *expects* unsteady corrections to be significant, and that the conclusion of Dudley and Ellington, that at no flight speed can the aerodynamics of the bumblebee be satisfactorily accounted for on steady-state principles, is as predicted on theoretical grounds.

A detailed, steady, lifting surface analysis of the wing of a house sparrow in mid-downstroke has been performed by Hummel and Mollenstadt (1977). Quite modest values of $\bar{C}_L =$ from 0.3–0.7 were reported, although the authors suggested that values of 0.7 are close to the maximum for such a wing profile at $Re_c \cong 10^4$. In general, blade element/quasi-steady lifting line methods will be valid for birds, bats and insects in steady forward flapping flight at sufficiently low Ω. The chief disadvantage is the requirement of, at least, detailed kinematic and morphological data, and preferably additional steady-state aerofoil measurements for a number of wing section profiles. The analysis can become cumbersome and tedious, and it may be difficult to generalise the results. Moreover, just what constitutes a small enough Ω remains unclear, as there are indications that $\Omega \approx 2.0$ is too high, even

from a rough, practical viewpoint. With further increases in Ω, the basic aerodynamic premises and assumptions are almost certainly invalid.

5.3 Momentum Jet

The momentum jet, or actuator disc model, is also a steady-state model, but it is a dramatic simplification of the situation (Fig. 12b). Nothing remains of the original animal apart from a circular disc, whose diameter is equal to the wingspan, $2b$. The disc applies a uniform downward acceleration to the fluid, which reaches a final vertical velocity of $2w_i$. The mass flux through the disc is $\rho U S_d$, and the rate of generation of downward momentum is the product of the mass flux times the velocity, $2w_i$, to which it is accelerated. In steady flight, this force balances the weight:

$$W = \rho U S_d \cdot 2w_i, \quad \text{or,} \quad w_i = \frac{W}{2\rho U S_d}. \tag{35}$$

The second expression gives a value for the induced velocity across the disc. It may be used as a first estimate to correct for the induced downwash in the blade element theory [Eq. (31)]. w_i is constant and so the power required to generate an upward force equal to the weight, W, is

$$P_i = W w_i = \frac{W^2}{2\rho U S_d e}. \tag{36}$$

e is the aerofoil efficiency introduced before, and it is used to account for the fact that air is not accelerated uniformly and steadily across S_d. Equation (36) is exactly equivalent to Eq. (11) derived from the lifting line equations, after substituting for the drag and lift coefficients, and noting that $S_d = \pi b^2$. There are no parameters which reflect the fact that the wings are actually beating, except indirectly via the increased thrust required to achieve the airspeed U.

Note how the perspective has changed, from considering the kinematics of the wingbeat and lifting properties of the aerofoil surfaces to calculating the momentum flux in the wake model, albeit a highly simplified one. The principal advantage of such a model is its simplicity and ease of manipulation. The power requirement can be calculated given only the body mass and the wingspan, and no other inputs are necessary. The disadvantage is that we may have thrown the baby out with the bath water; the model cannot reflect any changes in wing area, aspect ratio, wingbeat frequency, section geometry or kinematics, except by ad hoc adjustments of the factor e. Furthermore the wake model is not realistic.

5.4 Vortex Wake Models

Vortex Loops. In a sense, the momentum jet model is a vortex wake model; an infinitely thin, cylindrical sheet of vorticity surrounds the uniform jet, separating it from the outer undisturbed fluid. As w_i is spanwise constant there is no vorticity

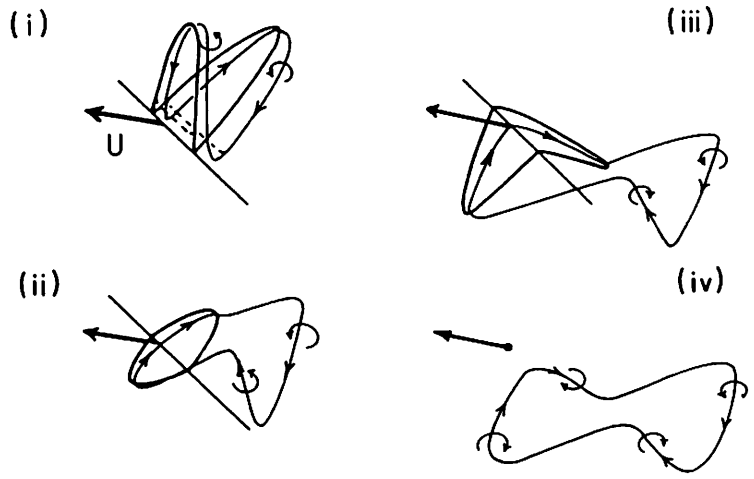

Fig. 13 (i)–(iv). A conjectural mechanism for the origin of a closed vortex loop behind a flapping wing pair. In each of the four timesteps, labelled frames (i)–(iv), the wing pair and wake are seen in oblique view, moving into the page with velocity U. The stick-like body takes no part in the aerodynamics. Vorticity shed during the downstroke is assumed to roll up immediately, and can therefore be represented as a single, curved line-vortex. The true behaviour of such a convoluted vortex is not known; here, local fluctuations in curvature decrease in magnitude with time. At the end of the downstroke, the wings vanish, since they contribute no further to force generation

inside the cylinder, which contracts in diameter as w_i increases. Figure 13 represents an attempt to construct a more realistic wake model from first principles, considering the motion of a rigid, beating wing pair on an infinitely thin body in steady forward motion. In the first frame, the wings are just beginning to move on the downstroke. According to the principles outlined in Sects. 3.1–3.2, the circulation at each span location, r, depends on the local chord, $c(r)$, and on the relative velocity, $\mathbf{u}(r)$, which, ignoring wake induced velocities for the moment, is the vector sum of the forward speed, U, and the local flapping velocity, $\mathbf{u}_w = 2\phi nr$. The local circulation may therefore fall towards the wing root, as indicated by the dotted lines in the wake, but if this $\delta\Gamma$ is assumed to be small, the starting vortex shed at the wing trailing edge could have an initial configuration something like frame (i). As the wings continue during the downstroke [frame (ii)], the tip vortices link the bound vorticity on the wing with the convoluted starting vortex which convects and deforms according to its own induced velocity field. At the end of the downstroke, the circulation on the wings drops to zero and a stopping vortex shed at the trailing edge completes a closed vortex loop which drifts away in the wake. Now, suppose the upstroke does no aerodynamic work whatsoever (the wings have disappeared in the last frame), and suppose that the loops of frame (iv) may reasonably be approximated as elliptical, planar, small-cored vortex rings. In this case, the wake is composed of a series of vortex loops, one created on every downstroke. This is the basis of the flight model for forward flight introduced by Rayner (1979a, b). The energy of each ring is determined by its size and circulation. The streamwise and spanwise ring dimensions are determined by the wingbeat kinematics and geometry, and by the form of $\Gamma(y)$ on the wings. The ring circulation is computed by enforcing the force balance condition that the rate of generation

of wake momentum must balance the vector sum of the weight and drags on the body and wings. The induced power is then calculated from the mean rate of increase of wake kinetic energy. The beauty of this calculation is that the details of wing profile geometries, spanwise twist, unsteady lift generation and vortex shedding in the wake are all unimportant – provided that the result is equivalent to a vortex loop with the predicted size. The unsteady effects are taken into account via the more realistic wake model, and the kinematic data requirements are not overwhelming. Moreover, the effect of varying ϕ and downstroke ratio, τ, could be investigated and related to the selection of flight style. It was found that variations in these parameters permitted access to a family of $P(U)$ curves, passing from small ϕ in fast flight, to large ϕ in the short, slow flights typical of small passerines, for example.

Independent confirmation that the wake can take the form of a series of closed vortex loops was provided by Kokshaysky (1979), from wake visualisation experiments on small passerines in a flight cage. Further quantitative work, using multiple-flash stereo photogrammetry and *3-D* wake reconstruction techniques (Spedding et al. 1984; Spedding 1986) showed that the only detectable concentrations of wake vorticity left in the wakes of the pigeon and jackdaw in slow flight were indeed almost-circular vortex rings (Fig. 14), but direct measurements of the wake momentum found only approximately half of that required for weight support. It was also demonstrated (Spedding 1986) that the wake circulation measurements were not internally self-consistent, implying that its structure, or time history, might be more complicated than suspected. This complexity is particularly evident in the initial and final roll-up of the convoluted vortex sheet [frames (i) & (iii)]. Mutual annihilation of viscous, finite-core vortices of opposite sign, followed by vortex reconnection, has been documented in interacting vortex rings, and it is reasonable to enquire whether it could occur so as to reduce the size and/or strength of the final, measured ring structure here. Saffman (1990) has

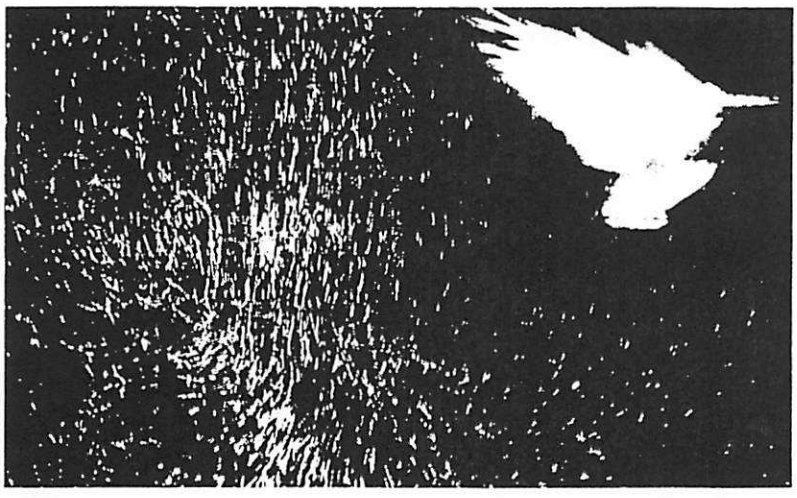

Fig. 14. Vortex ring in the wake of a slow flying pigeon. The flow is traced by multiflash images of neutrally buoyant, helium-filled soap bubbles

proposed a model which allows the time scales of these events to be estimated, governed by two parameters, ε and μ:

$$\varepsilon = \frac{a}{R}, \quad \mu = \frac{\pi \nu'}{\Gamma_0 \varepsilon^{1/2}}.$$

ε is the ratio of core radius, a, to ring radius, R, and μ is like an inverse Reynolds number, where $\nu' = 2\pi\nu$, and Γ_0 is the circulation. The characteristic times in seconds for cancellation and reconnection are T_c^* and T_r^*, respectively, estimated as:

$$\left.\begin{aligned} T_c^* &= \frac{5\pi R^2}{\Gamma_0} \varepsilon^{5/4} \left(\ln \frac{1}{\mu} \right)^{1/2} \\ T_r^* &= \frac{2\pi R^2}{\Gamma_0} \varepsilon^{1/2} \end{aligned}\right\}$$

Substituting the appropriate values for the pigeon wake, one arrives at time scales, $T_c^* \cong 0.4$s, and $T_r^* \cong 0.2$s, with the same order of magnitude as the stroke period ($T = 0.15$s). Initially, local regions of opposing, deformed loops will have smaller values of R, and consequently, shorter local time scales, T_c^* and T_r^*. The analysis is limited to cases where the separation distance, $z \ll R$. Firm conclusions cannot be drawn from this approximate analysis, but it does suggest that such viscous physical processes could significantly affect the dynamics.

A qualitatively similar wake structure has been reported in noctule and long-eared bats (Rayner et al. 1986), and together with Kokshaysky's result, it appears that this type of wake is characteristic of slow flight at high Ω ($\Omega = 5.8$ and 4.1 for the pigeon and jackdaw respectively) in birds and bats. Such a model predicts that less energy will be consumed by increasing the amplitude of the wingbeat, rather than the frequency, as U decreases, and this seems to be the strategy adopted in nature.

The closed-loop wake can only occur if the upstroke performs no aerodynamic work, and consequently leaves no trailing vortices. This is most simple to envisage in the slow flight of birds and bats when the wings are folded close to the body on the upstroke, whose function may be interpreted either as doing as little as possible (including minimising inertial and profile power requirements) for as short a time as possible, or as a means for effectively removing the bound vorticity built up on the wing during the downstroke. The upstroke often consumes a substantial fraction of the wingbeat period, and the latter interpretation may shed some light on the complex twisting and rotational motions. Insect wings cannot fold to the same extent during flight, and it is well established that they operate over both downstroke and upstroke (e.g. Jensen 1956; Vogel 1967; Nachtigall 1974), generating useful forces (with lift and/or thrust components) at either positive or negative angles of attack. The wake structure in this event will be different, the exact form depending on whether the starting and stopping vortices of successive wing strokes are merged or not (e.g. Brodskii and Ivanov 1984). Wake photographs behind a dragonfly in a wind tunnel (Azuma and Watanabe 1988) clearly show continuous tip vortices, but the cross-stream elements are hard to identify. Experiments by Luttges and co-workers (summarised in Luttges 1989) have demonstrated

complicated vortex wakes composed of a number of discrete coherent vortex structures behind tethered dragonflies and model wings in a wind-tunnel for values of Ω around 0.9–2.7, but one would be hard-pressed to formulate a general model based on such intricate smoke trail patterns. Presently, a vortex theory based on a simple wake model for forward flight in insects is lacking, although the LCM model, considered later, does incorporate a simple, fixed wake model into a blade element type of calculation.

There is no shortage of evidence from the wingbeat kinematics of both birds (e.g. Brown 1963) and bats (e.g. Norberg 1976a) in medium-speed flight, that at least part of the wing is aerodynamically active on the upstroke, and a conceptual model different from Fig. 13 is required.

The Roller-Coaster. As we have already remarked, the crucial requirement, in order to support the weight and provide thrust for steady forward flight, is that the wingstroke be, in some sense, asymmetric. The resultant aerodynamic force,

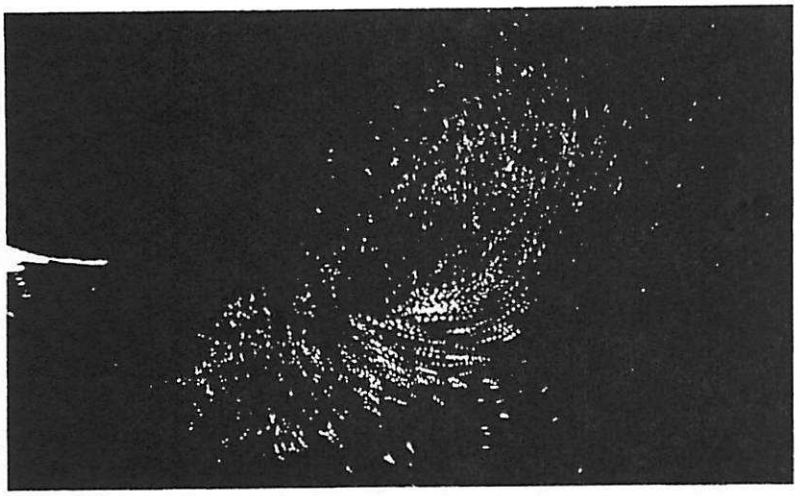

a

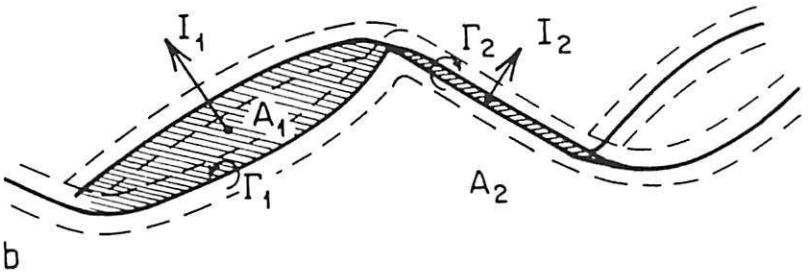

b

Fig. 15. **a** The wake of a kestrel in cruising flight. The flight was from right to left. The trailing vortex behind the starboard wing is marked by bubbles trapped inside the core. In the section created during mid-downstroke, the scarcity of bubbles has created a cutout, where the axial core flow, and behind this, the outer, induced, recirculating flow can be clearly seen. **b** Wake model based on **a**. Two line-vortices with constant circulation enclose planar areas A_1 and A_2 traced out by the extended wingtips, and folded primaries during the downstroke and upstroke, respectively

F, on a single beating wing with circulation distribution $\Gamma(y)$ over the semi-span, b, can be expressed as

$$\mathbf{F} = \rho \mathbf{u} \int_0^b \Gamma(y) dy, \tag{37}$$

and the orientation of **F** may be altered by changes in the wing stroke geometry, effectively changing the direction of **u**, while its magnitude may be modified via changes in $\Gamma(y)$, or in the semi-span, b. For any $\delta\Gamma$ on the wings, there must be an increment of $-\delta\Gamma_w$ in the wake, corresponding to the shedding of vorticity. If, on the other hand, b is gradually reduced, to b', say, while maintaining the same Γ_0, vortex shedding will be confined mostly to regions near the wingtips, where the largest adjustments in $\Gamma(y)$ occur, and the generation of concentrated spanwise vortices can be avoided. A nonzero net force may be generated according to the difference in impulse of the two segments of the wake. The wake of a kestrel in cruising flight has been shown (Spedding 1987b) to consist of two continuous undulating vortices, without detectable cross-connections between them, as confirmed by measurements of invariant circulation along the wake vortices. At the beginning and end of the flight, transverse starting and stopping vortices will be generated, thus completing the roller-coaster track. In cruising flight, the kestrel flexes the primary feathers on the upstroke, while the secondary feathers remain loaded, and the tip vortices appear to be shed at the corner between the two. Figure 15a shows an example wake photograph. Because the wake circulation, $\Gamma_w = \Gamma_0$, is constant, a very simple vortex wake model may be constructed, as in Fig. 15b, and the induced power requirement may be calculated from it. The impulses, $\mathbf{I}_1$ and $\mathbf{I}_2$, of the wake segments with areas A_1 and A_2, created during the downstroke and upstroke respectively are,

$$\mathbf{I}_1 = \rho\Gamma_0 A_1 \quad \text{and} \quad \mathbf{I}_2 = \rho\Gamma_0 A_2. \tag{38}$$

The reaction force is equal to the time rate of generation of the wake impulse, $\mathbf{F} = d\mathbf{I}/dt$, and so, if the planar wake segments make positive angles ψ_1 and ψ_2 with the horizontal, the average lift and thrust ($\equiv \bar{D}$ in steady, equilibrium flight) forces, integrated over one wingbeat period, T, are:

$$\left.\begin{aligned} \bar{L} &= \frac{1}{T}\rho\Gamma_0(A_1\cos\psi_1 + A_2\cos\psi_2) \\ \bar{D} &= \frac{1}{T}\rho\Gamma_0(A_1\sin\psi_1 - A_2\sin\psi_2) \end{aligned}\right\}. \tag{39}$$

The power requirement may be calculated by writing out the usual relationships for the force balance, when L must balance the weight minus any vertical components of the extra-lift drags, and D balances the remaining $\mathbf{D}_{par}$ and $\mathbf{D}_{pro}$ on the body and wings. If $\mathbf{D}_{pro}$ and $\mathbf{D}_{par}$ can be estimated, Eq. (39) can be solved for Γ_0 and one more unknown, which may be ψ, determined by the wingbeat kinematics, or $A_{1,2}$, determined also by the wing *shape*. The ratio of $A_1{:}A_2$ in Fig. 15 depends on the ratio of the flexed wingspan to the outstretched wing span, and since the span is reduced mostly by flexion of the primary feathers, simple

estimates of the flight performance can be calculated in terms of this ratio of wing planforms. For example, if $\psi_1 = \psi_2$, and the ratio of the upstroke to downstroke wake areas, $A_2/A_1 = \zeta$, ($\zeta \leqq 1$), then the lift: drag ratio may be expressed as

$$\frac{L}{D} = \left(\frac{1+\zeta}{1-\zeta}\right)\cot\psi. \tag{40}$$

L/D depends only on ζ and ψ, and it will increase with increasing ζ, and with decreasing ψ. When the L/D ratio is of concern, such as in long distance migration, the relationship above would predict that a sensible strategy would be to reduce the wing beat amplitude and flexion of the wing as far as is possible while still generating the required thrust. Alternatively, if ζ and ψ can be measured, then the values of L/D, or of D_{pro} and D_{par} implied or assumed in a flight model may be checked. Pennycuick (1989b) has done this to find significantly higher L/D ratios than predicted by simple actuator disc theory in the foraging flight of cormorants.

The roller-coaster model has a convenient balance between complexity and realism on the one hand, and simplicity and tractability on the other. The wingbeat amplitude and frequency and wing shape are represented as parameters affecting the wake shape, but since the circulation of the wake vortices is constant, the calculations are simple to perform. A comparable wake has been reported in the medium speed flight of bats (Rayner et al. 1986), and together with the observation that the cruising flight of a kestrel seems unremarkable and similar to that of many other birds in medium speed flight, it is likely that this wake structure (and hence valid application of the roller-coaster model) may be quite widespread. If the kinetic energy of the vortex wake essentially represents lost energy, then the roller-coaster wake without transverse vortex elements reflects a more efficient transport of material per unit distance than if the cross-stream elements were present. On these grounds, one might expect this wake to be present in *most* instances of long distance commuting or migrating flight.

Insect wings cannot flex in this fashion to reduce the wingspan, and so the required asymmetry must be achieved either from variations in the effective angle of attack, or the relative time of the down- and upstrokes. In either case, cross-stream vortices will be shed, and an accurate model should reflect this.

Swifts have curved, high aspect ratio, relatively rigid wings and may be unable to generate a roller-coaster wake. If so, their wings should be interpreted as extreme specialisations for soaring and high manoeuvrability, but perhaps accompanied by a different strategy for reduction of wake energy losses, via the parabolic lunate planform, which we shall discuss later. Hummingbirds have developed rigid wings with a low moment of inertia and extreme mobility of the shoulder joint, and their hovering flight resembles more that of insects than other birds. This specialisation for hovering apparently excludes them from the roller-coaster wake mode of flight, and is correlated with a rather limited record of nonstop migration. Altough the noctule of Rayner et al. (1986) was reported to be generating this wake, the limited ability of bats to reduce the wingspan beyond a minimum required for maintaining tension in the wing membrane, may also be predicted to limit their use of this mode flight, and correlates with a similar lack of notable migratory performance.

These issues have been discussed by Pennycuick (1988), who also speculates as to the possible wake patterns in extinct flying animals.

Rayner (1986) has incorporated this model wake structure into a quasi-steady lifting line analysis, where the form of $\Gamma(y)$ was taken to be that described by Jones (1980), and Γ_0 and ϕ were solved for a given frequency, n. $P(U)$ curves could be constructed from those combinations of n and ϕ that minimised the mechanical power requirement at each U. The inertial forces and wing root bending moments were also computed, and inertial components were found to be large, comparable to the aerodynamic forces in magnitude, as reported also by Bilo et al. (1984). Inertial power requirements have customarily been assumed to be negligible in forward flapping flight, but in the light of these results, this might not be correct for birds and bats executing large amplitude wing motions at low flight speeds.

5.5 Unsteady Lifting Line and Relatives

LCM. The Local Circulation Method has been developed and applied to the forward flight of dragonflies by Azuma et al. (1985) (LCM I), and refined by Azuma and Watanabe (1988) (LCM II). It combines the approach of the blade element analysis of wing sections with a more realistic and complete analysis of the modifying effects of the unsteady (time-varying) wake. The wing planform and initial circulation distribution is approximated by the superposition of a series of elliptical load distributions of diminishing size, each operating in the appropriate local shear flow. The wake model consists of the trailing and transverse (LCM II) vortices fixed by the path of the wing tip and trailing edge (Fig. 16a), and an iterative procedure is applied for the wake corrections to the circulation distribution, along the lines of Sect. 3.2. Nonlinear, empirical $c_l(\alpha)$ curves were used to compute the forces and moments on the wings at each blade element. Since the computations are quite lengthy, the wake attenuation coefficients were actually calculated only at $0.75R$.

The LCM I method was applied to the slow climbing flight of a dragonfly, for which k and Ω, as defined here, were approximately 1.6 and 16. Both wings operated well away from the linear $c_l(\alpha)$ range for a substantial portion of the wingstroke. The peak interference of the forewing wake on the hindwing was in mid-upstroke of the hindwing, and the wings operated with a phase difference so that the pitching moment was close to zero and a small net horizontal force was generated. First-order unsteady effects were accounted for and shown to be significant improvements over actuator disc-based estimates of constant downwash over the span, but no other special high-lift mechanisms requiring large scale separated flows were required to balance the forces in the analysis. The conclusions were similar for the LCM II study of the free flight of a dragonfly in a wind tunnel ($0.2 \leqq k \leqq 1.2$, $3.2 \leqq \Omega \leqq 12$). It is hard to gauge the significance of the additional corrections in LCM II since the two flight behaviours, and the reported curves of the total aerodynamic and inertial torques are quite different. The comparison of LCM II with a standard blade element calculation (constant w_i) at the highest flight speed, $U = 3.2\,\mathrm{m\,s^{-1}}$, and consequently lowest k and Ω ($= 0.2$ and 3.2)

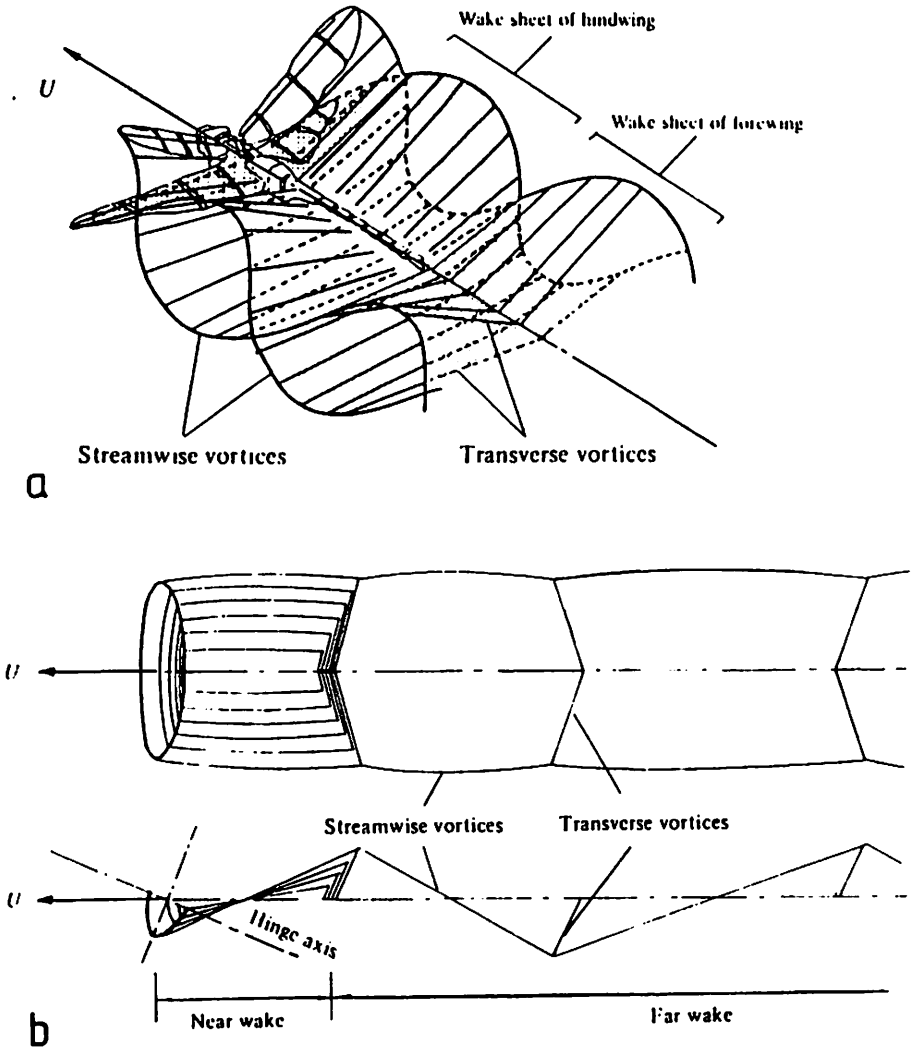

Fig. 16a, b. Vortex wake models for forward flapping flight. **a** Trailing and transverse vortices left in the path traced by the fore- and hindwings of the dragonfly. (Azuma and Watanabe 1988). **b** The near and far wake model. (Phlips et al. 1981)

revealed much smaller (around 20%) differences in the vertical forces than in the thrust (factors of 2–3), both for the instantaneous, and time-averaged values. Note that neither correction can be considered negligible. The estimated power requirements were well within the range for insect flight muscle.

Vortex Lattice and Lifting Line Methods. This group of techniques attempts to extend the standard lifting line of Sect. 3.3 to oscillating or flapping wings with geometry and kinematics closer to that found in nature. In contrast to the modified blade element approach, detailed kinematic data are not taken from experiment, but analytical forms of the planform geometry and wing motion are prescribed. Usually these take the form of linearised, small departures from the straight-edged, planar wing in steady motion, but the capacity to account for larger and more

realistic perturbations is growing with increasing sophistication of the analysis. The considerable advantage is that detailed parametric studies may be made of the effect of changing lifting surface geometries and kinematics. Also, the magnitude of the unsteady and *3-D* corrections to the quasi-steady analysis can be explicitly calculated, lending a more solid basis for the sometimes rather speculative discussions of the likely contributions of unsteady effects. Even when the strong nonlinearities of the true complex geometry and kinematics of natural flight exceed the domain of the model calculations, they can still provide a baseline estimate of the lower order effects, upon which further corrections can be superimposed. It is common to express the results in terms of the propulsive efficiency, $\eta \equiv U\langle T\rangle/\langle P\rangle$, where $\langle T\rangle$ and $\langle P\rangle$ are the time-averaged thrust, and the power required, respectively.

1. *Quasi-vortex lattice.* Lan (1979) formulated a version of a doublet lattice method for an oscillating flat plate wing, where, instead of representing a wing in steady uniform flow by a continuously-loaded lattice (Sect. 3.2), the oscillating surface was covered by a time-varying doublet lattice, and the system was solved for zero normal velocity at the lifting surface, as usual. When the pitch axis was fixed at the trailing edge, the sensitivity of a swept wing to phase differences in pitch and thrust was much reduced compared to an unswept rectangular wing. The swept wing always produced positive thrust while the rectangular wing occasionally produced a negative thrust i.e. a drag. This effect was more pronounced as k increased from 0.15 to 0.75. The interaction of pairs of rectangular wings oscillating in tandem was investigated, and the efficiency, η, and thrust coefficient, $\bar{C}_T$, were plotted as a function of phase difference, ϕ_{hf}, between the fore and hind wings, for different reduced frequencies and different gaps between the wing chords. ϕ_{hf} for optimum η and $\bar{C}_T$ decreased, both as k increased and as the separation distance decreased. On average, the predicted optimum ϕ_{hf} for energy extraction by the hindwings from the wake of the forewings was 45° and 90° for maximum $\bar{C}_T$ and η respectively. Azuma and Watanabe (1988) reported values of ϕ_{hf} between 51° and 93° for their dragonfly in free flight for $U = 0.7\,\mathrm{m\,s^{-1}}$ and $3.2\,\mathrm{m\,s^{-1}}$ respectively. The smaller ϕ_{hf} to maximise $\bar{C}_T$ rather than η is consistent with the changes in ϕ_{hf} of dragonflies in various flight maneouvres noted by Alexander (1984), and also with the qualitative trends reported by Ruppell (1989).
2. *2-D unsteady motion.* The basic principles of a high AR wing should be accessible to a *2-D* analysis, and detailed performance analysis and comparisons of *2-D* rigid and flexible aerofoils in unsteady motion have been made, following the lead of Lighthill (1970). These have been applied to problems of aero- and hydrodynamics, and the previous chapter may be consulted for further details. The more simple analysis allows a quite rigorous and thorough approach towards optimising the kinematics of the motion. Yates (1986) has considered in detail the optimum location for the pitch axis in a *2-D* analysis of a heaving and pitching fin or wing. The analysis included the physiologically inspired quantities of mean square pitching moment and mean square power requirement for maintenance of lift, which are of obvious relevance to animal flight. When

a mean lift force requirement was considered, the optimum pitch axis location always moved towards the quarter chord location. This corresponded closely to the presumed torsion axis at the location of the larger bones in vertebrate wings. Detailed static tests of torsional rigidity (Ennos 1988a, b) and estimation of the forces acting in Dipteran flight (Ennos 1989) indicate that the torsion axis typically lies at $0.15c$, while the centre of mass is located at about $0.3c$. It was noted that if the aerodynamic centre of presure is at $0.25c$, then local torques about the torsion axis will be created by both aerodynamic and inertial forces set up along the span during the wingbeat. The changes in local pitch could also explain the tip to base torsion waves observed in insect wings.

3. *Quasi-steady lifting line* ($k \ll 1$). Betteridge and Archer (1974) and Archer et al. (1979) applied the classical lifting line analysis to rigid and flexible wings in small amplitude flapping flight, and showed increased η with increasing k, and predicted high values of local wing twist, to maintain an elliptic loading profile. Based on similar model assumptions, Jones (1980) re-examined the optimum load distribution required to minimise the induced drag for a given wing root bending moment, and found that a 10% increase in thrust could be obtained, for the same η, for a $\Gamma(y)$ slightly reduced close to the base, and increased at the tip, compared to the elliptic distribution. Recall from Sect. 3.2 the preferred reduced tip loading for induced drag reduction in the steady lifting case. On these grounds, one would predict that specialised steady gliders/soarers will have more pointed wingtips than those that resort to flapping flight more often. This would appear to be the case, as we shall see in Fig. 18.
4. *3-D unsteady lifting line.* For the cases of most relevance to natural flight, a subset of three of the domains identified by Cheng (1976) in the asymptotic analysis can be identified for similar wings of high AR, characterised by the relative magnitudes of the chord length, c, the semi-span, b, and a wavelength in the wake, $\lambda = 2\pi U/\omega = \pi c/k$:

$$\begin{array}{lll} \text{I} & c \ll b \ll \lambda & \Omega \ll 1 \\ \text{II} & c \ll b = \mathrm{O}(\lambda) & \Omega = \mathrm{O}(1), \quad k \ll 1 \\ \text{III} & c = \mathrm{O}(\lambda) \ll b & k = \mathrm{O}(1). \end{array}$$

Domain I includes the limit as $\Omega \to 0$, and the flapping frequencies may be regarded as sufficiently small for the *3-D* problem to be treated as quasi-steady. In domain II, the flow next to the wing is nearly quasi-steady, while the velocity induced by the unsteady wake vorticity is as large as that induced by the trailing vortices. The roller-coaster kestrel wake was observed for $k = 0.26$, $\Omega = 2.32$, and we have already argued that this constitutes a range of some importance. Cheng and Murillo (1984) and Karpouzian et al. (1990) developed and examined the performance of an unsteady lifting line with centreline curvature for $\Omega = \mathrm{O}(1)$, showing that the balance of *3-D* corrections with the leading order thrust terms was responsible for an optimum degree of sweep (K_{opt}) for maximum η, when a reasonable, nonzero mean thrust was required. The difference in η between the *2-D* quasi-steady calculations, and those with *3-D* and unsteady corrections amounted to about 10% at K_{opt}, for $\Omega = 1.5$. Around these values of K, the parabolic lunate planform was

superior to a V-shape when no motion was allowed at the root. The identified optimum K would appear to be similar to the planforms of the swift and swallow families [Fig. 6(ii)], but this has not been rigorously checked. In domain III, Cheng (1976) showed that the global effects of the unsteady far wake were self-averaging, and that a *2-D* analysis is therefore superior for a straight wing (adding justification to the *2-D* investigations outlined above), but that local *3-D* corrections remained important for swept wings, as is true also of the quasi-steady domain I.

A *3-D* unsteady lifting line theory for planar, rigid, unswept wings of high AR has been developed by Phlips et al. (1981). It is based on a simplified model of the vortex wake, which is divided into near and far wake regions (Fig. 16b). Transverse vortices are shed at the extremes of the wingstroke, where they roll up, and are represented by a single line-vortex. Streamwise vortices are shed at the trailing edge and are assumed to remain in the path traced by the wings. In the far wake, they collect into trailing vortex lines. This model simplifies the calculation of wake induced velocities on the flapping wing, and the normal force on the wing can be calculated assuming the standard linear $c_l(\alpha)$ relation (Sect. 3.1). These assumptions effectively restrict the analysis to moderate values of k. When the wingbeat amplitude, ϕ, exceeded approximately 60°, significant departures from the steady state calculations were reported, particularly for $k > 1$. The effect of the induced velocity field in the unsteady calculation was to increase the value of the mean lift coefficient ($\approx 20\%$ for $\phi = \pi/2$, $k = 2$), but the mean thrust coefficients were reduced slightly, so that the efficiency, η fell with increasing k. This is a first order unsteady theory only, as spanwise flow along the wing and flow separation are ignored, but the clear implication is that unsteady terms cannot be neglected for $k \geqq 1$.

5.6 Unsteady Effects in Forward Flapping Flight

Some interim conclusions, summarising and generalising the results of the experimental and theoretical work above, can be stated. Note first that there are two contributors to unsteadiness in the aerodynamics. The first is that due to the kinematics of the lifting surfaces, and is measured by the frequency parameters k, Ω and K. The mean errors in time-averaged lift force, pitching moment, and aerodynamic torque calculations from quasi-steady analysis might be expected to be below 10% for $K \leqq 0.75$ ($J \geqq 1.5$), but *detailed* analysis and understanding of the effects of the wing kinematics and geometry require unsteady and *3-D* corrections in this domain, corresponding approximately to domain II above, where $k \ll 1$, $\Omega = O(1)$. In the cases of insect flight, ϕ varies little, and while the time-averaged corrections for $k \approx 0.1, \Omega \approx 1$ might be small, instantaneous forces and moments are unlikely to be correctly represented in the quasi-steady, *2-D* analysis. This covers most of the range of insect forward flight.

The second contributor to unsteadiness on the aerofoil comes from time varying shedding of vorticity at separation points on the lifting surface other than the trailing edge, about which the lifting-line models and current generation of

experimental techniques can say very little. Various high-lift mechanisms may be postulated, as in the hovering flight section, Sect. 6.4. Strongly separated flows could greatly affect the time-varying forces and moments on the wing. However, for the moment, the first order corrections due to the vortex wake can be used as lower bounds estimates for the unsteady effects. Azuma et al. (1985), using familiar logic, have argued that strongly separated flows need not be postulated for the dragonfly, as the forces balance correctly with only wake vortex corrections. Be that as it may, the actual details of the flow and the effects of unsteady separation on the instantaneous forces on a flapping animal wing for $k \geqq 0.1$ are not currently known with any great precision or certainty.

5.7 Flapping Flight Performance

The Aerodynamic Power Requirement. Just about any flight model generates a characteristic U-shaped curve of the total aerodynamic power requirement, P, with flight speed, U. The reasons for this may be found in Eq. (15), which in turn is based on the fundamental lifting-line analysis of Sect. 3.2. The combined profile drags on the wings and body increase by some constant times U^2 and so the power required, $P = DU$, rises with the third power of the velocity. By contrast, the induced drag is proportional to $1/U^2$. Any model – blade element, momentum jet, vortex ring, roller-coaster, LCM, unsteady lifting line – will consequently generate a generic, U-shaped power curve similar to Fig. 17, given some reasonable set of data, and the cost of transport, $C = P(mg \cdot U)$, will usually also possess a well-defined minimum. The references for each flight model may be consulted for detailed comparisons. Two general points may be made.

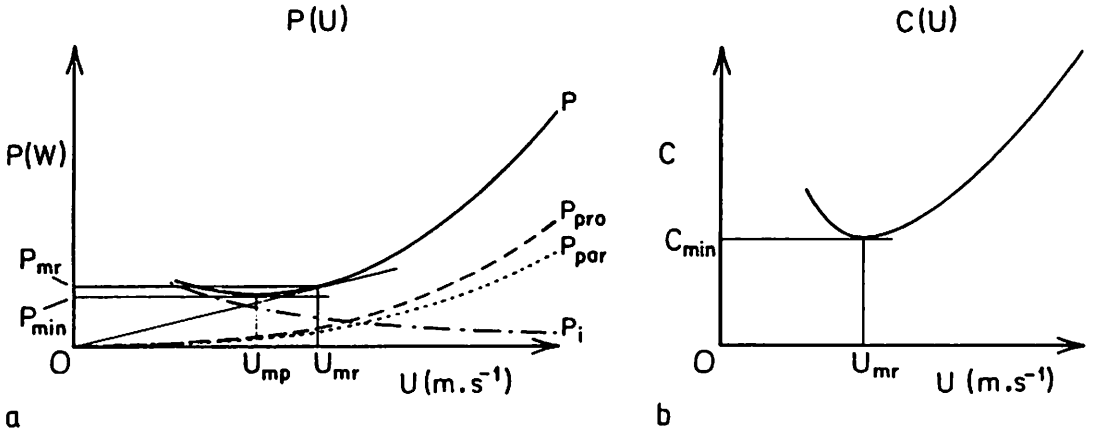

Fig. 17. **a** A generic power curve (this one was generated by the roller-coaster model for cruising kestrel flight). The total aerodynamic power, P, is the sum of the induced power, P_i, the profile power, P_{pro}, and the parasite power P_{par}. Variations in P_i between different models are usually small compared to differences in the calculation of P_{pro} and P_{par}. **b** The dimensionless cost of transport, C, has a well-defined minimum at U_{mr}

1. *Scale effects.* Equation (17) in Sect. 4.1 may be rearranged to show that a characteristic flight speed, such as that which maximises C_L, for example, is related to the square root of the wing loading, i.e.

$$U_{C_{L,max}} \propto \left(\frac{mg}{S}\right)^{1/2}.$$

In geometrically similar animals, since $m \sim l^3$ and $S \sim l^2$, then $U_{C_{L,max}} \sim l^{1/2}$. The dimensional power is $F.U$ and as $F \sim m$, then the mass-specific power requirement is also proportional to $l^{1/2}$. The maximum mass-specific power output of vertebrate and insect muscle actually decreases somewhat at contraction frequencies, $n < 10$ Hz (Weis-Fogh and Alexander 1977), and thus will decrease slightly with m, so at some size, the power required must exceed the power available from the flight muscles. The implications of these types of scaling relations have been explained by Penycuick (1975), who derived them from his momentum jet model. The power available, relative to any characteristic power requirement, is larger for small flying animals than larger ones. Small birds can hover or fly very slowly for small periods, while larger ones cannot. The larger birds have a very limited range of flight speeds available to them for continuous flapping flight, and show extreme specialisations for taking maximum advantage of gliding and soaring techniques. Deviation from geometric scaling, as larger gliding birds have higher aspect ratio wings, is clear in Fig. 18. Moreover, all the larger species in the left column of Fig. 18, albatrosses and the giant petrel, were found to possess a mechanical lock capable of resisting wing elevation above the horizontal. On the other end of the scale, a hummingbird with $m \cong 5$ g is capable of continuous aerobic hovering flight, although the largest of these, *Patagona gigas* ($m \cong 20$ g), appears barely capable of this. One should be wary of generalising across phyla, but these simple scaling laws are sufficient to account for the fact that almost all insects can hover continuously.

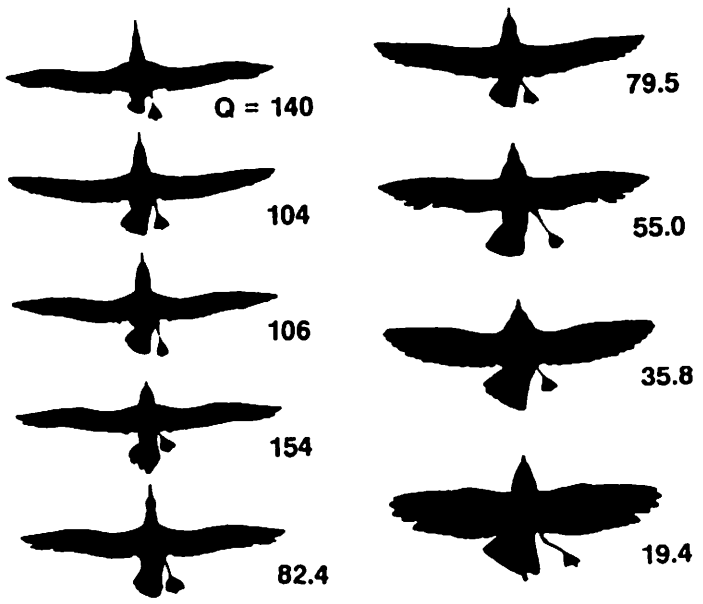

Fig. 18. Allometry in the wings of Procellariiformes. The outlines are rescaled by wingspan, $2b$. AR and $2b$ vary from 15 and 3 m in the wandering albatross at *top left*, to 8.04 and 0.39 m in Wilson's petrel. *bottom right*. The wing loading, Q, is shown for each species. (After Pennycuick 1982)

2. *The shape of the power curve.* The second point concerns the agreement between aerodynamic power requirements and metabolic measurements. In general, metabolic measurements result in U-shaped power curves (consult Norberg (1990) for a sample), but the shapes are often flatter than predicted. From the aerodynamics point of view, two potential contributors to such a trend might be noted: (1) *Re*-associated changes in the flow over the wings and/or body cause C_{Dpro}, C_{Dpar} to decrease significantly with U. (2) The flight style changes with U. (1) has been discussed in Sect. 3.1. Transition to turbulence around Re_{crit} can result in a strong inverse dependence of C_{Dpro} on U, and soaring birds appear to operate very close to that value. The most detailed measurements to date also indicate that, at high *Re*, C_{Dpar} is almost constant with increasing U, or falls slightly with *Re*. Even at the lower *Re* of insect flight, Dudley and Ellington (1990b) measured reductions in C_{Dpar} of approximately 40 and 25% as *Re* increased from 1×10^3 to 1×10^4, for body inclination angles (α_0) of 60° and 0° respectively, in their bumblebee experiment. The magnitude of the reduction and its dependence on α_0 is reasonably consistent with the expected behaviour of separated flows over bluff bodies at this *Re*. The result also suggests that changes in α_0 with U should be properly accounted for. (2) remains a possibility. D_{pro} on the wings could fall with increasing U if the wing span, $2b$, and so the wetted surface area, S_w, are reduced by the live animal, although the concomitant increase in D_i, together with associated changes in wing twist and local angle of attack, complicate the picture. While certain wingbeat parameters, such as the stroke amplitude ϕ, and the downstroke ratio, τ, are allowed, if not required, to vary with U in various flapping flight models (Rayner 1979b), others, such as the wingspan, b, are typically held fixed. The availability of families of glide polars with variable geometry wings is well established (Tucker 1987), but similar effects of systematic variations in wing planform geometry in flapping flight at different speeds have yet to be investigated. This could reduce the penalty for flight away from U_{mp} and would also contribute to scatter in the metabolic measurements. Both postulated mechanisms in (1) and (2) could flatten out the $P(U)$ curves, but the arguments remain essentially extrapolations from steady gliding to flapping flight, and so must be considered somewhat speculative. The remainder of the discussion is left to Chap. 8.

Kinematic and Behavioural Adaptations for Reducing Energy Consumption. Both the profile and parasite drags, together with the lift-induced drag, generate wake kinetic energy, and techniques to reduce the aerodynamic energy expenditure may be regarded as attempts to minimise this wake energy loss.

There are two simple *active* techniques (to be contrasted with *passive* measures such as improving streamlining) for reducing the total amount of energy deposited in the wake in the first place. They are undulating and bounding flight, both forms of intermittent flapping flight; in the former the wings are extended into the flow during the non-flapping stage and the animal glides, while in the latter they are folded tightly against the body. Both cases have been considered by Rayner (1985b). Bounding flight is quite simple to understand in principle. For small birds, especially those with large area, low aspect ratio wings, the wing profile drag

comprises a large fraction of the total aerodynamic drag, and at high flight speeds the increase in induced drag required to generate sufficient force for steady flight in only a portion of the wingbeat is more than offset by the significant reduction in wing drag during that time. For this to be a viable option, the flight speed must be high so the relative cost of induced drag is low. Careful considerations reveal several subtleties in the cost-benefit analysis, however, including the idea that muscle efficiency might be optimised at a fixed flapping frequency. Rayner's paper should be consulted for details. Bounding flight is common in passerines and also in hummingbirds, among others, but has not been recorded in bats. An intriguing variation on this theme has been reported by Betts and Wootton (1988) where the fast flying, low aspect ratio skipper butterfly (*Idmon* sp.) was reported to have its wings closed above the abdomen for $2T$ in intermittent flight.

A realistic analysis of undulating flight is quite complicated. It appears that when the wing loading is low and/or aspect ratio is high, it is more economical to alternate powered climbs, and gains in potential energy, with slower glides close to the minimum drag speed, than to fly at a constant flapping rate. This can be true when the maximum range speeds for flapping and gliding are different, and switching between the two is accompanied by potential and kinetic energy exchange. The allometric relationships manifest in Fig. 18 result in undulating flight being commonly observed in the larger seabirds, and it ought to be noted that this type of behaviour pattern also allows for the potential exploitation of updrafts, either in a systematic fashion such as when pelicans flap in the intervals between wave soaring, or on a more opportunistic basis. Undulating flight has been observed in bats (Thomas et al. 1990) and in butterflies (Betts and Wootton 1988), both of which have quite low wing loading.

There are further possibilities for energy extraction from the wakes of other flying colleagues by selecting a position such that the wing experiences the updraft created in their wakes, but not the downdraft (Lissaman and Schollenberger 1970; Hingdon and Corrsin 1978). Formation flight in birds has often been interpreted in this way, but the positioning accuracy required is quite considerable, and the likely benefits of attempting to track a complex undulating wake profile in flapping flight are not immediately obvious. One could perhaps consider the incentives to remain *away* from downdrafts, commensurate with the behavioural advantages of remaining in a flock, as restricting the domain of sensible locations. Formation flight has not been reported for insects.

Finally, the interaction of a trailing vortex pair with a wall boundary, such as the ground or sea surface, causes a reduction in the induced downwash on the wings, and consequently reduces the drag. The cancellation of normal velocities at the impermeable surface can be modelled by the addition of an imaginary mirror image vortex system an equal distance beneath the surface, where the induced velocities will therefore be exactly zero. For a simple horseshoe vortex, the ratio, R, of induced drag in ground effect to induced drag out of ground effect may be estimated by

$$R = \frac{C_{D_{i,g}}}{C_{D_i}} = \frac{(16H)^2}{(1 + 16H)^2}, \tag{41}$$

where $H = h/2b$ is the ratio of the flying height to wingspan. For entirely plausible values of H of around 0.2 (if $AR \approx 10$, this is 2 mean chord widths), $R \cong 0.6$, a substantial reduction. Aircraft must routinely take this into account on take-off and landing, and various sea birds, such as brown pelicans, clearly profit by flying at or below these values of H. Hainsworth (1988) has measured typical gliding heights of pelicans in ground effect, and Blake (1983) has discussed the topic with reference to bird flight in some detail.

6 Hovering

6.1 The Flow Regime

Hovering flight can be defined as the ability to remain airborne in a fluid with zero or negligible mean relative velocity between the body and the fluid. Since the forward speed of the body contributes nothing to the flow over the wings, hovering is the most energetically demanding of flight styles. From the scaling arguments presented in the forward flight analysis, this mode of flight will clearly be restricted to smaller flying animals, mostly insects and hummingbirds, and the latter may be considered as honorary insects for our purposes. Momentary hovering is typically unavoidable in landing and take-off and must be accomplished by most flying animals that cannot rely on special mechanisms involving either the storage of potential energy (dropping from a height) or the extraction of reliable sources of kinetic energy in the environment (soaring). Hovering and slow forward flight have been instrumental in enabling insects to occupy microniches not available to larger flying animals. From an analytical perspective, some simplifications arise since the form drag on the body may be neglected, but the importance of accurate estimates of the lift-induced power, and by implication, realistic models of the wake vorticity distribution, is greatly increased.

Hovering flight may be defined as all cases where $\Omega \geqq 20$, following the pragmatic example of Ellington (1984, III). Since the reduced frequency parameter Ω is infinite when $U = 0$, it is no longer particularly helpful in distinguishing amongst the different hovering regimes. A dimensionless amplitude may be defined by the number of mean chord lengths travelled by the mid-point on the wing, $R/2$:

$$\bar{\Lambda} \equiv \frac{\phi R}{2\bar{c}}. \tag{42}$$

This is also a measure of the mean distance of a wing chord from the unsteady influence of its own starting vortex. Similarly, the instantaneous position from the starting point at the end of a half-cycle can be expressed as the ratio, $\lambda = \gamma r/c$. In comparisons with *2-D* experiments, we let $\Lambda = h/c$, where h is the oscillation amplitude of a chord motion given by $x = h \sin \omega t$.

6.2 Quasi-Steady Analysis

Normal Hovering. To provide weight support to the animal, there has to be a horizontal component of the wing motion, and in the absence of any net horizontal body motion, the wings themselves must therefore beat in a horizontal plane. Acting within the mechanical constraints of the musculo-skeletal system, the simplest way of achieving this is for the body to tilt toward the vertical, and this indeed is the mode of hovering for hummingbirds and for several orders of insects analysed in classic papers by Weis-Fogh (1972, 1973) and Ellington (1984, I–VI). Figure 19 shows the course of one wingbeat cycle in a hovering sphingid moth. The time is spent approximately equally on the morphological up- and downstrokes, at the ends of which the wings twist and rotate so that the stiffened anterior part of the wing functions as the aerodynamic leading edge throughout. The wing motion relative to the body is often assumed to follow a figure-of-eight path, as reported for the hummingbird (Stople and Zimmer 1939), but the measurements of Ellington (1984, III) on the kinematics of insects *in free flight* show that this is not always so. Weis-Fogh (1973) introduced some very elegant simplifications to the basic blade element analysis leading to Eq. (34). The instantaneous lift δL on a wing section (blade element) δS can be expressed as:

$$\delta L(r,t) = \tfrac{1}{2}\rho \times C_L(r,t) \times \delta S(r) \times r^2 \left(\frac{d\gamma}{dt}\right)^2. \tag{43}$$

First, based on observations of the kinematics, C_L was assumed to be constant over both the span, R, and over the stroke period, T. δS is determined by the

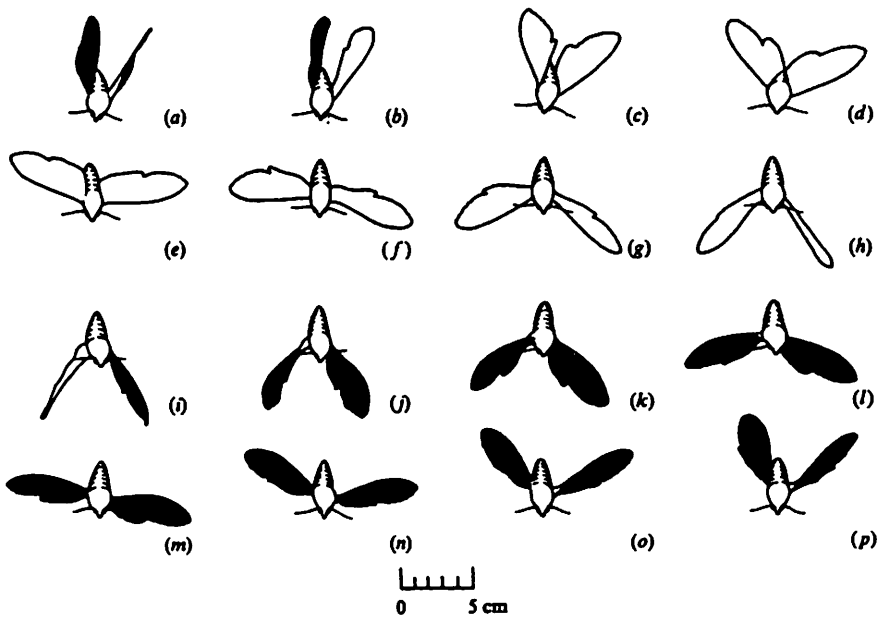

Fig. 19a–p. Normal hovering in *Manduca sexta*, as traced from every 10th frame of high speed cinefilm at ≅ 3450 frames s^{-1}. The view is from above, and the undersides of the wings are in *black*. (Weis-Fogh 1973)

second moment of area of the wing, for which analytical expressions were derived for simple wing shapes. The mean lift over one wing stroke is thus

$$\bar{L} = \tfrac{1}{8}\rho\omega^2\phi^2\bar{C}_L \times \int_0^R c(r)r^2\,dr + \frac{1}{T}\int_0^T \cos^2\omega t\,dt, \tag{44}$$

and the first integral is equal to σcR^3, where σ is the wing shape factor, and the second evaluates exactly to 1/2. Since $\bar{L}$ must balance half the weight if there are two wings, the mean lift coefficient is

$$\bar{C}_L = \frac{8W}{\rho\omega^2\phi^2\sigma cR^3}. \tag{45}$$

This is an extremely simple expression for estimating the mean lift coefficient required to support the weight of a hovering animal, given just the kinematic parameters in the denominator. In the majority of cases, normal hovering could be satisfactorily explained on steady-state principles, and the required lift coefficients appeared to be quite modest (from 0.8 at Re_c 1600, to 1.2 at Re_c 6700). However, all of the cases where the wingbeat was inclined significantly from the horizontal required abnormally large values of $\bar{C}_L$ and the steady state hypothesis had to be rejected. This included the bat *Plecotus auritus*, the butterfly *Pieris napi*, the hoverflies (Syrphinae) and the now famous chalcid wasp, *Encarsia formosa*.

These arguments have been re-evaluated by Ellington (1984, I–VI), based on meticulous kinematic and morphological measurements. In addition to pointing out certain methodological inconsistencies, he noted that the ladybird (*Coccinella 7-punctata*) and the crane-fly (*Tipula obsoleta*) would require mean lift coefficients of 1.7 and 1.2, respectively, too high at $Re_c \cong 10^3$. However, the measured wingbeat kinematics *were* consistent with postulated *unsteady* mechanisms for extra lift generation. Now, since the kinematics of these two species were not appreciably different from the others, which nevertheless had plausible $\bar{C}_L$ values, the steady-state explanation seems suspect for those as well. This argument, which is only strengthened when we recall that the calculated $\bar{C}_L$ values are *mean* values over the whole stroke, and that maximum values would have to be higher still, leads to the *opposite* conclusion, namely that *most* hovering animals make considerable use of unsteady rotational lift generation mechanisms. There are even broader implications because the insufficiency of the proof by contradiction method has clearly been exposed – it cannot be used to show that unsteady mechanisms are of no importance, it can only *fail* to show, on occasion, that steady-state aerodynamics are adequate.

Inclined Stroke Plane. Hovering in birds and bats is accomplished by beating the wings on an inclined stroke plane (Norberg 1976b; Dathe et al. 1984). The wingtip traces out a path with an average angle of 20–30° to the horizontal, and the wing is flexed and folded during the upstroke so that, although the upstroke may generate some lift (Dathe and Oehme 1978) it is much less than on the downstroke, and a crucial asymmetry is introduced into the contribution to weight support.

Table 1. Mean downstroke lift coefficients and dimensionless amplitudes for horizontal and inclined stroke plane hovering

Species	Reference	β(degrees)	$\bar{C}_{La}$	$\bar{\Lambda}$
Bombus hortorum	EL84	−15	1.1	3.4
Episyrphus balteatus (HF07)	EL84	−2	1.17	3.4
(HF08)		21	3.93	2.3
(HF08)		32	5.08	2.4
Aeschna juncea	NA75	60	3-4*	2.5
Amazilia f.f	WF72	11	2.3*	3.6
Ficedula hypoleuca	NU75	30	6.0*	1.98
Columba livia	DA82	38	2.6	4.6
Larus ridibundus	DA82	41	2.0	4.4
Plecotus auritus	NU76	30	4.3*	3.2

References: WF82, Weis-Fogh (1972); EL84, Ellington (1984, VI); NA75, R. Norberg (1975); NU75, U. Norberg (1975); DA82 Dathe (1982); NU76, U. Norberg (1976b). The asterisked quantities were recalculated in Ellington (1984).

In insects, inclined stroke plane hovering is characteristic of hoverflies and dragonflies, where α_{eff} can remain high on the upstroke, but the vertical component of **F** will still be reduced. Conventional aerodynamic analysis shows that this places unreasonable demands on the lifting performance of the wing on the downstroke, so that all animals using inclined stroke plane hovering must rely to some extent on unsteady lift generation mechanisms. Table 1 summarises some data from the literature and shows that estimated lift coefficients are uncomfortably or impossibly high wherever ß increases much beyond 15°. The value of 2.3 recalculated by Ellington for the hummingbird in the horizontal stroke plane suggests that here too the quasi-steady analysis fails.

6.3 Vortex Models

Theory. Specifically to remedy the deficiencies in the quasi-steady analysis, Ellington (1978, 1980) introduced and refined (1984, V) a vortex theory of hovering flight. The principle is to construct a reasonable and solvable mathematical model of the wake vorticity distribution, based on the wing beat kinematics. The wake must be allowed to convect with its own self-induced velocity, and the mechanical power requirement is then computed from the mean rate of increase of wake kinetic energy. The procedure is actually quite similar to that of the original momentum jet model, only now a more accurate wake model is required. There are two obvious corrections to be made to the steady, uniform momentum jet: (1) spatial corrections to account for the fact that the wings do not sweep over the whole disc area, and,

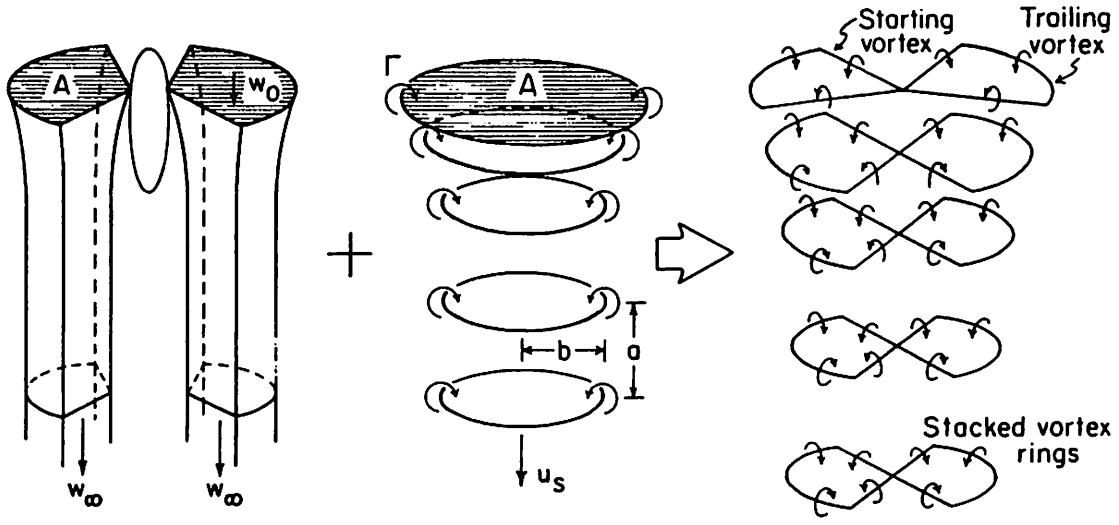

Fig. 20. The nonuniformities in space and time of the vortex wake of a hovering animal are modelled by the superposition of two independent corrections to the uniform momentum jet. (Assembled from Ellington 1978, 1980)

(2) temporal corrections to include the time-varying circulation distribution. In the limit of a wing pair beating through an angle of 2π, at an infinite frequency, we should recover the ideal momentum jet. A simplified illustration of these corrections is given in Fig. 20. Physically, since vorticity can only be created at the wing surface, and since the wings are oscillating in time with angular velocities falling to zero twice per wingbeat (when vorticity must be shed into the wake), the wake should be composed of a series of stacked, closed vortex loops, one completed beneath each wing on every half-cycle. Mathematically, the first order effect of these two small perturbations can be expressed as the addition of two linearly independent corrections to the steady momentum jet model for the power:

$$\bar{P}_i = \bar{P}_{i,mom}(1 + \sigma + \tau). \tag{46}$$

σ is a *spatial* correction which depends on the ratio of circulation required to support the weight over the area actually swept by the wings ($A_0 = \phi R^2 \cos\beta$), to the circulation required if the whole disc ($A = \pi R^2$) were used. It is a positive constant, vanishing to zero when $A_0 = A$. τ is a *temporal* correction which may be expressed as $0.079s^2$, where s is a parameter defining the wake element spacing, related to the ratio of the distances a/b in Fig. 20. When the spacing is zero, the wake is continuous and τ is zero also. Ellington (1984, V) should be consulted for details. There are two immediate benefits from this analysis. First, one has a method for calculating the induced power which takes reasonable account of unsteady aerodynamic effects because it is based on a reasonable model of the vortex wake. This analysis does not require assumptions concerning quasi-steady section lift coefficients. Second, a more accurate estimate of the true induced velocities and explicit corrections to the steady-state models enable *quantitative* estimates of the effect of these steady-state assumptions to be made. Ellington estimated that the

corrections were around 20% for normal hovering, and up to 60% for the inclined stroke plane cases.

Rayner (1979c) formulated a model for hovering animal flight based on a wake of stacked, coaxial, small-cored vortex rings. Provided that the core radius is small compared to the ring radius, the system is effectively determined by two parameters; the feathering parameter, $f = w_i^2/|\mathbf{u}_t|^2$ is the square of the ratio of the steady induced velocity in the momentum jet to the mean wingtip velocity, and, typically, is almost an order of magnitude smaller in insects than in birds. R' is a measure of the ring size with respect to the span, b; it depends on $\Gamma(y)$ on the wing, and also on the area actually swept out by the wings, i.e. on ϕ. Reasonable values seem to be around 0.75. The correction σ_0 to the actuator disc induced power requirement ($P_i = \sigma_0 P_{i,mom}$) could be written

$$\sigma_0 = \frac{0.95}{R'} + \frac{1.2}{R'^5} f. \tag{47}$$

For insects, σ_0 is close to 1, and corrections to the steady momentum jet model were estimated to be typically 10–15%. Calculations for Norberg's *Ficedula* data, on the other hand, showed $\sigma_0 = 1.8$, a considerable difference from the momentum jet model, implying significantly increased wake energy losses. This is related to the increased wake element spacing, which in turn derives from the inactive morphological upstroke. The implication is that "avian" hovering places unattainable demands on the aerobic power output of the flight muscles of most birds, which, therefore, do not hover, except momentarily. In general, where the vortex models of Ellington and Rayner overlap, as in the case of hovering insect flight, the numerical results and conclusions are quite similar. A detailed comparison appears in Ellington (1984, V).

It should be noted that the vortex wake models are not free of assumptions and simplifications. Although it is true that no steady-state wing section lift coefficients need be invoked, the generation of the wake elements with a certain size, R', say, with respect to the wing shape and kinematics *does* implicitly assume a certain circulation distribution on the wing in order to create this pattern of wake vorticity. This capacity for ignoring the complex details of the circulation and lift on the wing itself is precisely one of the strengths of vortex wake models, but the validity of the assumed wing circulation or core vorticity distributions is difficult to confirm. In view of the problems in interpreting the existing quantitative wake velocity measurements, the presumed roll-up of shed vorticity into simple wake elements with predicted R' cannot yet be regarded as verified. Despite these reservations though, the closed vortex loop wake models are easily the most realistic, solvable, formulations available for slow and hovering flight, and overall corrections due to complex wake geometries and deformations may yet prove to be small.

Experiment. Maxworthy (1979) constructed a simple *3-D* mechanical model of a pair of rigid wings which rotated through an angle of 2π in a horizontal plane, like an idealised hovering wing pair (the geometry is similar to the insert of Fig. 21). When the wings start and finish pressed together, the final structure in the wake

is a large vortex ring, with a smaller one of opposite-signed circulation inside it, shed from the inboard trailing edge of each wing. This, together with observations of vortex rings in the wakes of birds in slow flight, indicates that complete vortex rings may result when the stroke amplitude, ϕ, is high. On the other hand, when the wing tapers to very small chord lengths at the root, or is separated from the body by a small gap, there is likely to be strong vortex shedding in the neighbourhood of the root, where the normal velocities are also small. Dathe et al. (1984) have observed single closed vortex loops beneath models of isolated rectangular wings beating in a horizontal plane, and this is to be expected when there is no possibility of mutual wing interference effects. In this respect, the flow is just as postulated in Ellington's vortex model, and will probably be the form of the wake when ϕ is small so that the wings operate in effective isolation, such as in the inclined stroke plane hovering of the hoverflies, for example.

It is extremely hard to visualise the wake of a real hovering animal. Ellington (1978, 1980) presented streak photographs of a tethered crane-fly (*Tipula paludosa*) and a butterfly (*Pieris brassicae*). Large vortex-dominated motions can be distinguished over the wings of *Pieris*, but the *Tipula* wake structure was indistinct. Coherent vortex structures could be seen in phase-averaged photographs of neurogenically forced wing motions in tethered dragonflies (*Libelluala luctuosa*) by Somps and Luttges (1985), but the overall picture was incomplete.

If the vortex theories can confirm that unsteady mechanisms must be operating in nearly all cases of hovering flight, they do not indicate what those mechanisms might be. In the absence of definitive experimental evidence from the real animal, physical mechanisms must be postulated based on the known behaviour of fluids, or on mechanical models.

6.4 High-Lift Mechanisms

Dynamic Stall. An impulsively started aerofoil must move through more than four chord lengths to reach 80% of the asymptotic circulation. This is known as the Wagner effect, which reduces the lift initially available to an accelerating wing (cf. Chow and Huang (1982) for solutions for flat-plate and finite thickness aerofoils, and Auerbach (1987) on the difficulties in satisfactory modelling of even this geometrically-simple, separated flow). If, however, the aerofoil is started at a geometric angle of attack higher than the steady-state stalling angle, α_{crit}, large transient circulations can be built up during the first few chord lengths of travel, when the lift exceeds the steady-state values. Both rotational and translational accelerations can produce this effect up until $\lambda \approx 4$. Dynamic stall (see McCroskey (1982) for a review) may be accompanied by leading edge separation and flow reattachment before the trailing edge, forming a separation bubble whose increase in circulation is added to the normal wing circulation. Eventually, the bubble moves away and convects downstream over the wing surface, with a very sharp drop in lift, but if the wing is oscillating continuously, the unsteady forces may remain favourable through much of the cycle. Favier et al. (1982) have shown that coupled, in-phase variations in U and α ($\Delta U \cong 0.68U$; $\Delta\alpha = 6°$) of an accelerating and pitching aerofoil produced *mean* lift coefficients over the oscillation cycle of 2.66 times the steady-state value, for $k = 0.59$, $\Lambda = 0.57$, and $Re_c = 8 \times 10^4$.

At lower Re_c, stall is less abrupt, and useful lift can be generated even at high α, so dynamic stall mechanisms might be less effective. However, the phenomenon of flow separation at a sharp edge is almost Re-independent. Large local decelerations in the flow and high concentrations of vorticity at the surface can cause separation even at $Re < 0.1$. The initial shear layer instability is inviscid, and while viscous effects dominate in the separated region itself, affecting stability and reattachment of the flow there, roll-up of the shed vorticity will still occur. Maxworthy's (1979) experiments on model wings showed almost identical separated flows at $Re_\omega \cong 30$ and $Re_\omega \cong 10^4$ ($Re_\omega = \dot{\gamma}c^2/\nu$) although the vortex cores were noncircular at the lower Re_ω. This spans almost the entire range of Re of interest in insect flight. The flow visualisations of impulsively started aerofoils at $16 < Re_a < 5.2 \times 10^4$ ($Re_a = \dot{v}^{1/2}c^{3/2}/\nu$) by Freymuth (1985) clearly demonstrate that the onset of flow separation is not particularly dependent on Re, even from a smooth profile, although the shape and structure of the separation vortices themselves can vary dramatically.

Wing rotation and acceleration at the ends of the wingbeat are likely to be of great importance in hovering flight over a broad range of length scales. Even when mean steady state lift coefficients appear adequate, they could not be achieved without some means of avoiding the Wagner effect, most likely through some dynamic stall process.

Wing Interference. Apart from the alteration of the effective incidence angle due to the unsteady induced flow from previous wingbeats, there are two possible mechanisms for wing interference in a solitary hovering animal. The first involves interactions between opposing wings as they approach one another at the ends of the wing strokes. An extreme example of this was discussed by Weis-Fogh (1973) and Lighthill (1973) based on wing motions observed in *Encarsia formosa*, which apparently operated with $\bar{C}_L \cong 2.3$, an impossible feat for steady aerofoils at $Re_c = 20$. The wing kinematics were distingushed by an unusually prolonged "clap" phase at the end of the upstroke, when the dorsal wing surfaces were pressed together. When they opened on the subsequent downstroke, they did so by rotation about their trailing edges which remained connected until the including angle approached 120°, when they parted with opposing sections translating away from each other. Air rushing into the opening gap could produce very large circulations around each wing, without any vortex shedding, since the circulation around each wing was equal in magnitude and opposite in sign, and the total around both wings (which were still connected) was still zero! This surprising result, a new *inviscid* mechanism of lift generation, showed that high instantaneous lift forces would be generated by such flows, and was consistent with the observed vertical accelerations of the body. The experiments of Maxworthy (1979), numerical simulations by Haussling (1979), and theoretical analysis by Edwards and Cheng (1982) revealed that very large separation vortices would be generated at the sharp leading edge, significantly enhancing the circulation, which continued to increase, even beyond including angles of 120°. Calculations from instantaneous force measurements and simultaneous quantitative flow visualisations over an opening wing pair at $Re_\omega = 3 \times 10^3$ by Spedding and Maxworthy (1986), showed *mean* lift coefficients of 6.9–8.5 over the wing opening time. It was not necessary for the wings

to be completely closed to achieve this result. Significant performance enhancements are clearly achievable, though the wing opening time history can strongly affect the growth of circulation in the separation vortex, which is turbulent at this *Re*.

Ellington (1980, 1984, IV) has commented on the likely modifications of the basic clap and fling mechanics due to wing flexibility and departures from the idealised rigid wing kinematics, and Fig. 21a shows two wing sections approaching, but not touching, and then peeling apart as the wings flex when the leading edge initially begins to rotate. In the second variation (Fig. 21b), the wings meet at the trailing edge, but never at the leading edge, and separation is again preceded by a flexible peel motion. The available but incomplete experimental evidence suggests that these mechanisms ought to be successful in producing high unsteady lift forces, and that this type of motion is quite widespread in nature. The near or partial clap and fling motions of many birds and bats in take-off and landing manoeuvres and of many insects in hovering and rapidly accelerating flight may ultimately be crucial for the success of these species, which perform many wingbeats of essentially steady flight, but also absolutely depend on the ability to occasionally generate high transient lift forces.

The second case of wing interference is specific to insects and concerns the interaction between fore- and hindwing pairs. Wing interference was calculated to

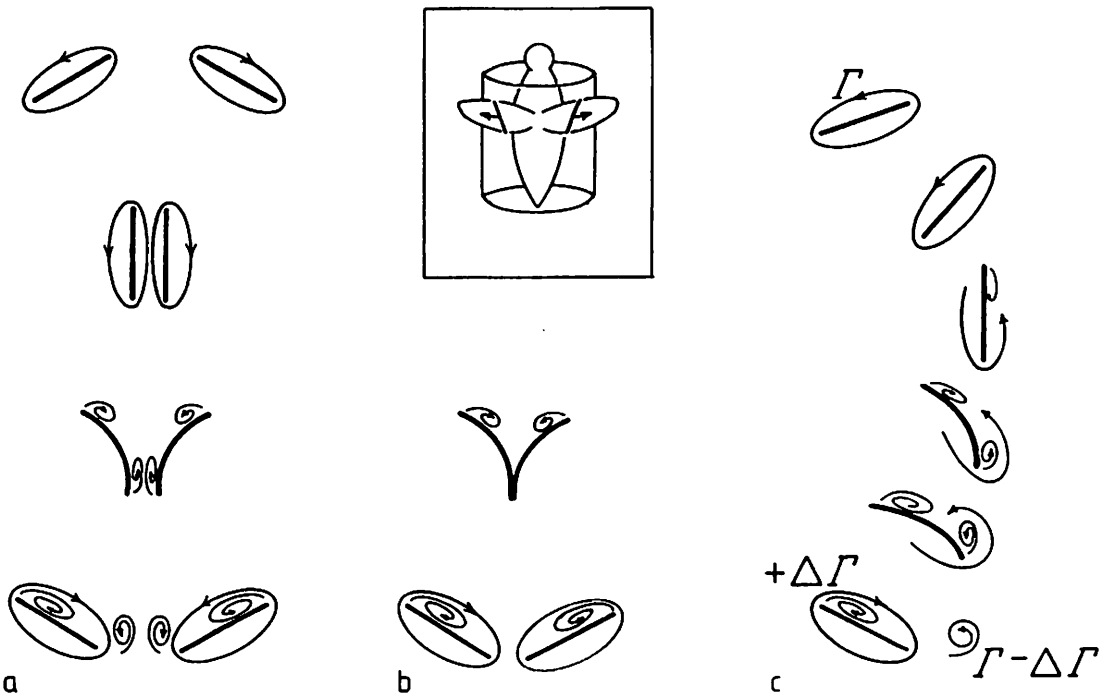

Fig. 21 a–c. Unsteady lift generation mechanisms. The plane of section is normal to the long axis of the wings, which thus appear as chord sections. If the wings beat in a horizontal plane, then the sections lie on the surface of an imaginary vertical cylinder which intersects the wings at mid-span (*inset*). **a** and **b** Modified versions of the clap and fling motion. **c** The flex mechanism for an isolated wing in rotation. (Ellington 1984, IV)

be responsible for only 2% corrections in Jensen's (1956) analysis of locust flight, but the phase relations between wing pairs in dragonflies nevertheless appear to conform to theoretical predictions based on optimised wake energy extraction (Sect. 5.4). Reavis and Luttges (1988) measured the lift and drag forces on a tethered dragonfly and correlated them with simultaneous flow visualisations. Leading edge separation vortices were produced over both wings and those produced by the forewing convected downstream to interact with the hindwing. Interpretation of the force records is complicated somewhat by the fact that the inertial contribution, which Azuma and Watanabe (1988) have demonstrated may be equal in magnitude to the aerodynamic force, cannot be isolated. Extremely complex flows were described by Saharon and Luttges (1989) for mechanical models of dragonfly wing pairs, and lift and thrust control were interpreted from the varying wing-vortex interactions produced with different phase angle differences. According to this view, both the magnitude and direction of the aerodynamic forces are dominated by the interaction of the lifting surfaces with coherent vortices shed during different phases of the wingbeat.

Isolated Rotation. From the discussion of dynamic stall, it is clear that single wings in isolation may generate high transient lift values by rotation alone. The most plausible mechanism has been suggested by Ellington (1984, IV), coined the "flex" (Fig. 21c). Consider a wing section towards the end of a stroke (top of the figure). Various arguments have been advanced that it is likely to have a separation bubble generated by rotational acceleration at the beginning of the stroke. Since the circulation must be reversed in sign before the next stroke, this vorticity must be shed with the same sign as the starting vortex for the next stroke. If the wing rotates as it decelerates towards the end of the stroke until the section is almost vertical, there will be vortex shedding, but now of opposite sign at the leading edge, while the circulation from the separation bubble is left around the trailing edge. If the wing rotates about this trailing edge, a new separation bubble may be formed at the leading edge without the generation of extra circulation at the stationary trailing edge. The previous separation vortex appears as a combined starting and stopping vortex. The wing flexion appears to make such kinematics possible for the hoverflies observed by Ellington, although all that is really required is that rotation should occur about the stationary trailing edge. Since the starting and stopping vortices are combined, a hoverer using the flex mechanism should have half as many wake vortices as one which does not, and they should be spaced twice as far apart in the vertical direction. The correction σ to the induced power requirement in Eq. (46) should be similarly affected, as the wake energy losses are reduced. Freymuth (1990) has published photographs of the wake of a *2-D* flat plate in combined translation and pitching oscillations, and one of his modes of oscillation is similar to that of Fig. 21c for a rigid plate rotating about the trailing edge. Figure 22 is redrawn based on his photographs. It is unfortunate that the flow over the surface cannot be seen, but the starting and stopping vortices of successive strokes are obviously combined during this motion. For $\Lambda = 3$ and $Re_\Lambda = \omega \Lambda c^2/\nu = 1.7 \times 10^3$, lift coefficients of 2.5–3 were estimated from the time averaged jet impulse. This is quite strong, though not conclusive, evidence for the

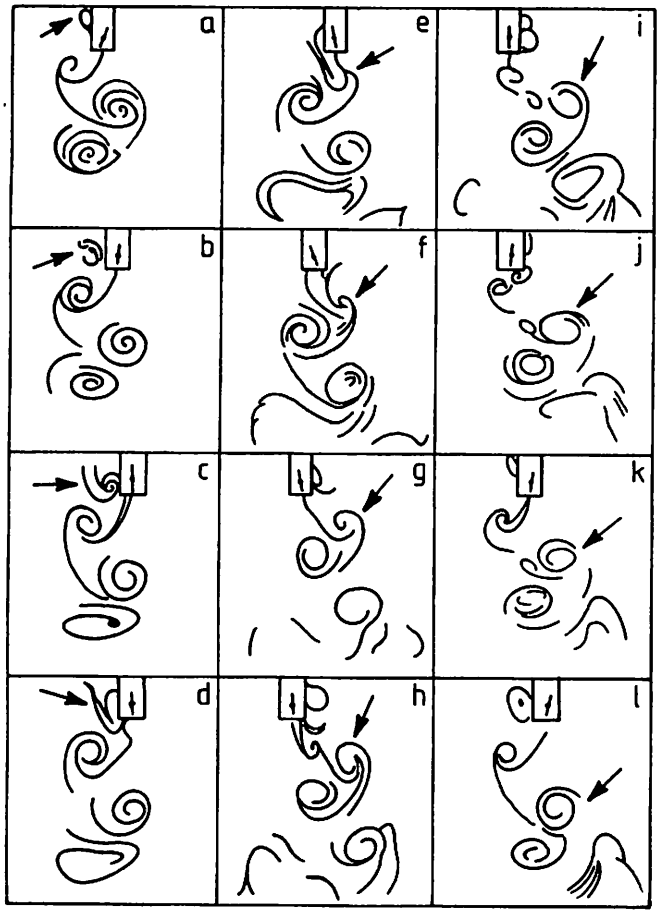

Fig. 22a–l. The wake of a rigid *2-D* plate in oscillating pitch and translation. The first frame is in mid-stroke, moving from left to right, and the time sequence proceeds by column for one complete oscillation cycle. The *arrow* follows the life history of a single vortex which begins as a leading edge vortex (**a–c**), and ends as a combined starting and stopping vortex (**f, g**), convecting away in the far wake thereafter. The plate itself could not be seen as it is obscured by the mounting strut, whose rectangular shilhouette is shown in outline here. The line inside this is a rough estimate of the location and orientation of the plate, based on information elsewhere in the paper. The pitching and heaving motions are combined with a 90° difference in phase so that rotation occurs approximately about the trailing edge at the ends of each stroke. The lines in the flow represent concentrations of $TiCl_4$ which originates on the surface of the plate, as does the vorticity. $\Lambda = 0.5$, $Re_\Lambda = 340$. (Redrawn from photographs in Freymuth 1990)

practicability of Ellington's flex mechanism, and it would be interesting to see clear quantitative demonstrations of this.

6.5 Power Requirements

The total mechanical power required for hovering flight is the sum of the power required to produce the aerodynamic forces,

$$\bar{P}_a = \bar{P}_i + \bar{P}_{pro}, \tag{48}$$

together with the power required to accelerate the wings to and fro during the wingbeat. This will have two components, one to accelerate the second moment of the wing mass, m_2, and the other to accelerate the second moment of the virtual mass, v_2, which is related to the mass of the air influenced by the accelerating wing. The virtual wing mass is usually calculated from the mass of an imaginary cylinder of air with diameter equal to the wing chord and length equal to R. The mean, mass-specific power required to accelerate the wing at the beginning of a wing stroke thus has the form,

$$\bar{P}^*_{acc} = \frac{\omega}{\pi}(m_2 + v_2)\left(\frac{d\phi}{dt}\right)^2_{max} \Big/ mg. \tag{49}$$

In the analysis of forward flight, this term was ignored since $d\phi/dt$ is usually small, but this is no longer true for hovering flight. Moreover, no useful net forces can be derived from this equation as $d\phi/dt$ is zero when averaged over the whole wingbeat cycle. Unfortunately, decelerating wings still require positive expenditure of metabolic energy, albeit only 1/10th of that required to accelerate them in the first place. If we make a charitable assumption that the deceleration occurs almost free of charge, then, in the absence of any elastic energy storage mechanism, the total specific power required is

$$\bar{P}^* = \bar{P}^*_a + 2\bar{P}^*_{acc}. \tag{50}$$

from the components in Eqs. (48) and (49). If there were perfect elastic energy storage, the kinetic energy of the wings would be converted at the end of every wing stroke to elastic strain energy, which would be returned to reaccelerate the wings on the following stroke, and $\bar{P}^*$ would equal $\bar{P}^*_a$ alone. Ellington calculated that $\bar{P}^*_a$ for his hovering insects was 17–19 W N^{-1}. If the maximum power output of insect fibrillar muscle is roughly that of vertebrate striated muscle, then the maximum specific power available is about 26 W N^{-1} (Weis-Fogh and Alexander 1977). This leaves almost no margin for accelerating the wings. Since this power requirement is large, estimated to be $\bar{P}^*_{acc} \approx 1.4\text{–}5.9\,\bar{P}^*_a$, there must be substantial elastic energy storage in hovering insect flight. Given the small power margin, the elastic efficiency must also be high. Deformations of the cuticular thoracic box, and of the protein resilin, and passive stretching of the fibrillar flight muscles all provide possible elastic storage mechanisms in insects, but equivalents do not appear to have been developed by vertebrates. Calculations similar to these for Weis-Fogh's hummingbird, *Amazilia*, indicated that without elastic storage [i.e. using the full form of Eq. (50)], the mechanical power requirement was about 21 W N^{-1}, which would require a conversion efficiency of around 24%. This is an entirely reasonable result, and it also indicates that the flight of hummingbirds is dominated by inertial power requirements. At high contraction rates, elastin has high internal damping and is not suitable as an elastic resonator (Weis-Fogh 1972), and the apparent failure of vertebrates to evolve a substitute has probably considerably limited their access to motions involving high frequency oscillation. Hummingbirds may well represent the practical limit. On the other hand, the same aerodynamic analysis leads to the conclusion that the considerable success of

insects in slow or hovering flight, and the exploitation of microenvironments is due in significant measure to the combined elastic properties of the flight musculature, exoskeleton and specialised protein rubbers.

7 Concluding Remarks

This chapter has reviewed the current state of knowledge concerning aerodynamic mechanisms in animal flight, by examining the various analytical models and their predictions and consequences. These provide a framework within which the evolution and adaptation of natural flight systems can be understood. There is considerable scope for refinement and improvement of many of the model techniques, but even the simplest, the venerable actuator disc, has been shown to be successful, as judged by the ability to make useful, testable predictions of behaviour and morphology.

It is hoped that the steady/unsteady debate has now run its course. The broad spectrum of aerodynamic mechanisms and analytical techniques is poorly represented by insisting on a binary classification. Progress in theory and experiment in the last 10 years has allowed the problem to be recast in a more physical and mathematically-precise fashion, and the aerodynamic effects of the unsteady *kinematic* and *3-D* corrections have been explicitly calculated over a large fraction of the parameter space relevant to animal flight. In many cases, it ought to be possible to attempt an estimate of the magnitude (and sign) of at least the first order corrections. It does not seem unreasonable that these numerical estimates could be used to generate families of possible power curves, or curves with error bars or envelopes. Such calculations are conspicuously rare in the literature.

On the other hand, establishing the role of the dynamics of viscous-inviscid interactions in the boundary-layer and strongly separated regions is of critical importance. Fluctuating or periodic growth and bursting of separation regions is another source of unsteadiness in the flow (as opposed to the kinematics, measured by k, Ω). Related to this point, there is a clear need for further quantitative investigations of the fluid dynamics of simple bodies in the Reynolds number range 10^1–10^5, with rotational and translational accelerations appropriate for animal flight. In keeping with the introductory comments on scientific models, results for the most basic shapes are the more generalisable, starting with *2-D* flat plates. The accurate determination of the normal pressure and skin friction drags, even on simple fixed bodies and wing shapes, also remains a major stumbling block and source of uncertainity in the aerodynamic calculations.

Much remains to be discovered concerning time varying separated flows, stability and control, the effects of flexibility and porosity of membranous and feathered surfaces, and the role of passive and active changes in geometry of real animal wings. Aspects of manoeuvrability and agility, structural robustness and damage repair have also been neglected here. Some of these phenomena may be of interest only to a small number of fluid dynamicists, while others will have

profound consequences for the balance of energetics of the organism. Ultimately the correct sorting category can only be assigned when the details are known sufficiently for accurate model simulations.

Note. An electronic accompaniment to this chapter is available in the form of *Mathematica* notebooks where analytical and numerical examples of the model equations may be manipulated and plotted. Readers interested in receiving a copy are invited to send a formatted Macintosh disc to the author.

Acknowledgments. I would like to thank my friends and colleagues, Professors FK Browand and HK Cheng for their diligent reviews of an earlier draft of this article.

References

Alexander DE (1984) Unusual phase relationships between the forewings and hindwings in flying dragonflies. J Exp Biol 109: 379–383

Althaus D (1980) Profilpolaren fur den Modelflug. NeckarVerlag, Karlsruhe

Anderson JD (1984) Fundamentals of Aerodynamics. McGraw-Hill, NY

Archer RD, Sapuppo J, Betteridge DS (1979) Propulsion characteristics of flapping wings. Aero J 83: 355–371

Auerbach D (1987) Experiments on the trajectory and circulation of the starting vortex. J Fluid Mech 183: 185–198

Azuma A, Azuma S, Watanabe I, Furuta T (1985) Flight mechanics of a dragonfly. J Exp Biol 116: 79–107

Azuma A, Watanabe T (1988) Flight performance of a dragonfly. J Exp Biol 137: 221–252

Batchelor GK (1967) An Introduction to Fluid Dynamics. Cambridge Univ Press, Cambridge

Betteridge DS, Archer RD (1974) A study of the mechanics of flapping wings. Aero Q 25: 129 141

Betts CR, Wootton RJ (1988) Wing shape and flight behaviour in butterflies (Lepidoptera: Papilonoidea and Hesperioidea): a preliminary analysis. J Exp Biol 136: 271–288

Bilo D, Lauck A, Nachtigall W (1985) Measurement of linear body accelerations and calculation of the instantaneous aerodynamic lift and thrust in a pigeon flying in a wind tunnel. Biona Rep 4: 87–108

Blake RW (1983) Mechanics of gliding in birds with special reference to the influence of the ground effect. J Biomech 16: 649–654

Brodskii AK, Ivanov VD (1984) The role of vortices in insect flight. Zool Theor 63: 197–208

Brown RHJ (1963) The forward flight of birds. Biol Rev 38: 460–489

Burkett CW (1989) Reductions in induced drag by the use of aft swept wing tips. Aero J 93: 400–405

Caple G, Balda RP, Willis WR (1983) The physics of leaping animals and the evolution of preflight. Am Nat 121: 455–467

Cheng HK (1976) On lifting-line theory in unsteady aerodynamics. Univ So Cal Aero Eng Rep USCAE 133

Cheng HK (1985) Laminar separation from airfoils beyond trailing-edge stall. Univ So Cal Aero Eng Rep USCAE 141

Cheng HK, Murillo LE (1984) Lunate-tail swimming propulsion as a problem of curved lifting line in unsteady flow. Part 1. Asymptotic theory. J Fluid Mech 143: 327 350

Cheng HK, Smith FT (1982) The influence of airfoil thickness and Reynolds number on separation. J Appl Math Phys (ZAMP) 33: 151–180

Chow C-Y, Huang M-K (1982) The initial lift and drag of an impulsively started airfoil of finite thickness. J Fluid Mech 118: 393 409

Cloupeau M, Devillers JF, Devezeau D (1979) Direct measurements of instantaneous lift in desert locust; comparison with Jensen's experiments on detached wings. J Exp Biol 80: 1 15

Cone CD (1962a) The theory of induced lift and minimum induced drag of nonplanar lifting systems. NASA TR R-139
Cone CD (1962b) Thermal soaring of birds. Am Sci 50: 180–209
Cone CD (1964) A mathematical analysis of the dynamic soaring flight of the albatross. V Inst Mar Sci SSR 50: 1–104
Csicsaky M (1977) Body gliding in the zebra finch. Fortschr Zool 24: 275
Dathe HH (1982) Efficiency calculations on the hovering flight of the pigeon (*Columba livia*) and the black-headed gull (*Larus ridibundus*). Zool Jb Physiol 86: 209–242
Dathe HH, Oehme H (1978) Typen des Ruttelfluges der Vogel. Biol Zbl 97: 299–306
Dathe HH, Oehme H, Kitzing H (1984) On the configuration of the wake of hovering birds. Zool Jb Physiol 88: 387–403
Dudley R, Ellington CP (1990a) Mechanics of forward flight in bumblebees. I. Kinematics and morphology. J Exp Biol 148: 19–52
Dudley R, Ellington CP (1990b) Mechanics of forward flight in bumblebees. II. Quasi-steady lift and power requirements. J Exp Biol 148: 53–88
Edwards RH, Cheng HK (1982) The separation vortex in the Weis-Fogh circulation-generation mechanism. J Fluid Mech 120: 463–473
Ellington CP (1978) The aerodynamics of normal hovering flight: three approaches. In Schmidt-Nielsen K, Bolis L, Maddrell SHP (eds) Comparative Physiology – water, ions and fluid mechanics. Cambridge Univ Press, Cambridge, pp 327–345
Ellington CP (1980) Vortices and hovering flight. In: Nachtigall W (ed) Instationare Effekte an schwingenden Tierflugeln. Steiner, Wiesbaden, pp 64–101
Ellington CP (1984) The aerodynamics of hovering insect flight. I. The quasisteady analysis. II. Morphological parameters. III. Kinematics. IV. Aerodynamic mechanisms. V. A vortex theory. VI. Lift and power requirements. Phil Trans R Soc Lond B 305: 1–181
Ennos AR (1988a) The importance of torsion in the design of insect wings. J Exp Biol 140: 137–160
Ennos AR (1988b) The inertial cause of wing rotation in Diptera. J Exp Biol 140: 161–169
Ennos AR (1989) Inertial and aerodynamic torques on the wings of Diptera in flight. J Exp Biol 142: 87–95
Ennos AR, Wootton RJ (1989) Functional wing morphology and aerodynamics of *Panorpa germanica* (Insecta:Mecoptera). J Exp Biol 143: 267–284
Favier D, Maresca C, Rebont J (1982) Dynamic stall due to fluctuations of velocity and incidence. AIAA J 20: 865–871
Freymuth P (1985) The vortex patterns of dynamic separation: a parametric and comparative study. Prog Aerospace Sci 22: 161–208
Freymuth P (1990) Thrust generation by an airfoil in hover modes. Exp Fluid 9: 17–24
Hainsworth FR (1988) Induced drag savings from ground effect and formation flight in brown pelicans. J Exp Biol 135: 431–444
Haussling HJ (1979) Boundary-fitted coordinates for accurate numerical solution of multibody flow problems. J Comp Phys 30: 107–124
Hertel H (1966) Structure, Form and Movement. Reinhold, NY
Herzog K (1968) Anatomie und Flugbiologie der Vogel. Fischer, Stuttgart
Higdon JJL, Corrsin S (1978) Induced drag of a bird flock. Am Nat 112: 727–744
Hummel D, Mollenstadt W (1977) On the calculation of the aerodynamic forces acting on a house sparrow (*Passer domesticus*) during downstroke by means of aerodynamic theory. Fortschr Zool 24: 235–256
Ito A (1989) The effect of trailing edge extensions on the performance of the Gottingen 797 and the Wortmann FX 63-137 aerofoil sections at Reynolds numbers between 3×10^5 and 1×10^6. Aero J 93: 283–289
Jensen M (1956) Biology and physics of locust flight. III. The aerodynamics of locust flight. Phil Trans R Soc Lond B 239: 511–552
Jones RT (1980) Wing flapping with minimum energy. Aero J 84: 214–217
Jones RT (1990) Wing Theory. Princeton Univ Press, Princeton
Karpouzian G, Spedding GR, Cheng HK (1990) Lunate-tail swimming propulsion. Part 2. Performance analysis. J Fluid Mech 210: 329–351
Kokshaysky NV (1979) Tracing the wake of a flying bird. Nature (Lond) 279: 146–148
Lan CE (1979) The unsteady quasi-vortex-lattice method with applications to animal propulsion. J Fluid Mech 93: 747–765

Lee CJ, Cheng HK (1990) An airfoil theory of bifurcating laminar separation from thin obstacles. J Fluid Mech 216: 255–284
Liebeck RH (1978) Design of subsonic airfoils for high lift. J Aircraft 15: 547–561
Lighthill MJ (1969) Hydromechanics of aquatic animal propulsion – a survey. Ann Rev Fluid Mech 1: 413–446
Lighthill MJ (1970) Aquatic animal propulsion of high hydromechanical efficiency. J Fluid Mech 44: 265–301
Lighthill MJ (1973) On the Weis-Fogh mechanism of lift generation. J Fluid Mech 60: 1–17
Lighthill MJ (1975) Mathematical Biofluiddynamics. Chapter 8: Animal flight. SIAM, PA, pp 151–178
Lighthill MJ (1977) Introduction to the scaling of aerial locomotion. In: Pedley TJ (ed) Scale effects in animal locomotion.Academic Press, London, pp 365–404
Lissaman PBS (1983) Low-Reynolds-numbers airfoils. Ann Rev Fluid Mech 15: 223–239
Lissaman PBS, Schollenberger CA (1970) Formation flight of birds. Science 168: 1003–1005
Lugt HJ (1983) Vortex Flow in Nature and Technology. Wiley, NY
Luttges MW (1989) Accomplished insect fliers. I: Gad-el-Hak M (ed) Frontiers in experimental fluid mechanics. Lecture Notes in Engineering 46. Springer, Berlin Heidelberg New York Tokyo, pp 429–456
Maxworthy T (1979) Experiments on the Weis-Fogh mechanism of lift generation by insects in hovering flight. Part 1. Dynamics of the 'fling'. J Fluid Mech 93: 47 63
McCroskey WJ (1982) Unsteady airfoils. Ann Rev Fluid Mech 14: 285–311
Nachtigall W (1974) Insects in Flight. McGraw-Hill, NY
Nachtigall W (1977) Die aerodynamische Polare des Tipula-Flugels und eine Einrichtung zur halbautomatischen Polarenaufnahme. In: Nachtigall W (ed) The Physiology of Movement; Biomechanics. Fisher, Stuttgart, pp 347–352
Nachtigall W (1979) Der Taubenflugel in Gleitflugstellung: Geometrische Kenngrossen der Flugprofile und Luftkrafterzeugung. J Orn 120: 30–40
Newman BG, Savage SB, Schouella D (1977) Model tests on a wing section of an *Aeschna* dragonfly. In: Pedley TJ (ed) Scale effects in animal locomotion. Academic Press, London, pp 445 477
Norberg RA (1975) Hovering flight of the dragonfly *Aeschna juncea* L., kinematics and aerodynamics. In: Wu TY, Brokaw CJ, Brennen C (eds) Swimming and Flying in Nature, vol 2. Plenum Press, NY, pp 763–781
Norberg UM (1975) Hovering flight in the pied flycatcher (*Ficedula hypoleuca*). In: Wu TY, Brokaw CJ, Bennen C (eds) Swimming and Flying in Nature, vol 2. Plenum Press, NY, pp 869–881
Norberg UM (1976a) Aerodynamics, kinematics, and energetics of horizontal flapping flight in the long-eared bat *Plecotus auritus*. J Exp Biol 65: 179–212
Norberg UM (1976b) Aerodynamics of hovering flight in the long-eared bat *Plecotus auritus*. J Exp Biol 65: 459–470
Norberg UM (1985) Evolution of vertebrate flight: an aerodynamic model for the transition from gliding to active flight. Am Nat 126: 303–327
Norberg UM (1990) Vertebrate Flight. Springer, Berlin Heidelberg New York Tokyo
Norberg UM, Rayner JMV (1987) Ecological morphology and flight in bats (Mammalia; Chiroptera): wing adaptations, flight performance, foraging strategy and echolocation. Phil Trans R Soc Lond B 316: 335–427
Oehme H, Kitzler U (1975) Untersuchungen zur Flugbiophysik und Flugphysiologie der Vogel. II Zur Geometrie des Vogelflügels. Zool Jb Phys 79: 402–424
Pennycuick CJ (1968) A wind-tunnel study of gliding flight in the pigeon *Columba livia*. J Exp Biol 49: 509 526
Pennycuick CJ (1971a) Gliding flight of the dog-faced bat *Rousettus aegyptiacus* observed in a wind tunnel. J Exp Biol 55: 833–845
Pennycuick CJ (1971b) Gliding flight of the white-backed vulture *Gyps africanus*. J Exp Biol 55: 13–38
Pennycuick CJ (1973) Wing profile shape in a fruit-bat gliding in a wind tunnel, determined by photogrammetry. Period Biol 75: 77 82

Pennycuick CJ (1975) Mechanics of flight. In: Farner DS, King JR (eds) Avian Biology, vol 5. Academic Press, London, pp 1 75
Pennycuick CJ (1982) The flight of petrels and albatrosses (Procellariiformes), observed in South Georgia and its vicinity. Phil Trans R Soc Lond B 300: 75–106
Pennycuick CJ (1983) Thermal soaring compared in three dissimilar tropical bird species, *Fregata magnificens*, *Pelecanus occidentials* and *Coragyps atratus*. J Exp Biol 102: 307–325
Pennycuick CJ (1986) Mechanical constraints on the evolution of flight. In: Padian K (ed) The Origin of Birds and the Evolution of Flight. Mem Cal Acad Sci 8: 83–98
Pennycuick CJ (1987b) Flight of seabirds. In: Croxall JP (ed) Seabirds: feeling biology and role in marine ecosystems. Cambridge Univ Press, Cambridge, pp 43–62
Pennycuick CJ (1988) On the reconstruction of pterosaurs and their manner of flight, with notes on vortex wakes. Biol Rev 63: 299–331
Pennycuick CJ (1989a) Bird Flight Performance. A Practical Calculation Manual. Oxford Univ Press
Pennycuick CJ (1989b) Span-ratio analysis used to estimate effective lift: drag ratio in the double-crested cormorant *Phalacrocorax auritus* from field observations. J Exp Biol 142: 1–15
Pennycuick CJ, Obrecht HH, Fuller MR (1988) Empirical estimates of body drag of large waterfowl and raptors. J Exp Biol 135: 253–264
Phlips PJ, East RA, Pratt NH (1981) An unsteady lifting line theory of flapping wings with application to the forward flight of birds. J Fluid Mech 112: 97–125
Rayner JMV (1979a) A vortex theory of animal flight. II. The forward flight of birds. J Fluid Mech 91: 731–763
Rayner JMV (1979b) A new approach to animal flight mechanics. J Exp Biol 80: 17 54
Rayner JMV (1979c) A vortex theory of animal flight. I. The vortex wake of a hovering animal. J Fluid Mech 91: 697–730
Rayner JMV (1985a) Mechanical and ecological constraints on flight evolution. In: Hecht MK, Ostrom JH, Viohl G, Wellnhofer P (eds) The Beginnings of Birds. Proc Int Archeopteryx Conf, Eichstatt, pp 279–288
Rayner JMV (1985b) Bounding and undulating flight in birds. J Theor Biol 117: 47–77
Rayner JMV (1986) Vertebrate flapping flight mechanics and aerodynamics, and the evolution of flight in bats. Biona Rep 5: 27–74
Rayner JMV (1988) Form and function in avian flight. In: Johnstone RF (ed) Current Ornithology, vol 5. Plenum Press, NY, pp 1–66
Rayner JMV, Jones G, Thomas A (1986) Vortex flow visualisations reveal change in upstroke function with flight speed in bats. Nature (Lond) 321: 162–164
Reavis MA, Luttges MW (1988) Aerodynamic forces produced by a dragonfly. AIAA-88-0330
Rees CJC (1975a) Form and function in corrugated insect wings. Nature (Lond) 256: 200–203
Rees CJC (1975b) Aerodynamic properties of an insect wing section and a smooth aerofoil compared. Nature (Lond) 258: 141–142
Ruppell G (1989) Kinematic analysis of symmetrical flight manoeuvres of Odonata. J Exp Biol 144: 13–42
Saffman PG (1990) A model of vortex reconnection. J Fluid Mech 212: 395–402
Saharon D, Luttges MW (1989) Dragonfly unsteady aerodynamics: the role of the wing phase relations in controlling the produced flows. AIAA-89-0832
Schmitz FW (1960) Aerodynamik des Flugmodells. Lange, Duisberg
Somps C, Luttges M (1985) Dragonfly flight: novel uses of unsteady separated flows. Science 228: 1326–1329
Spedding GR (1986) The wake of a jackdaw (*Corvus monedula*) in slow flight. J Exp Biol 125: 287–307
Spedding GR (1987a) The wake of a kestrel (*Falco tinnunculus*) in gliding flight. J Exp Biol 127: 45 57
Spedding GR (1987b) The wake of a kestrel (*Falco tinnunculus*) in flapping flight. J Exp Biol 127: 59–78
Spedding GR, Maxworthy T (1986) The generation of circulation and lift in a rigid two-dimensional fling. J Fluid Mech 165: 247 272
Spedding GR, Rayner JMV, Pennycuick CJ (1984) Momentum and energy in the wake of a pigeon (*Columba livia*) in slow flight. J Exp Biol 111: 81 102

Spillman JJ (1987) Wing tip sails; progress to date and future developments. Aero J 91: 445–453
Stolpe M, Zimmer K (1939) Der Schwirrflug des Kolibri im Zeitlupenfilm. J Orn Lpz 87: 136–155
Thomas ALR, Jones G, Rayner JMV, Hughes PM (1990) Intermittent gliding flight in the pipistrelle bat (*Pipistrellus pipistrellus*) (Chiroptera: Vespertilionidae). J Exp Biol 149: 407–416
Tucker VA (1987) Gliding birds: the effect of variable wing span. J Exp Biol 133: 33–58
Tucker VA (1990) Body drag, feather drag and interference drag of the mounting strut in a peregrine falcon, *Falco peregrinus*. J Exp Biol 149: 449–468
Tucker VA, Heine C (1990) Aerodynamics of gliding flight in a Harris' hawk, *Parabuteo unicintus*. J Exp Biol 149: 469–489
Vogel S (1967) Flight in *Drosophila*. III Aerodynamic characteristics of fly wings and wing models. J Exp Biol 46: 431–443
Vogel S (1981) Life in Moving Fluids: the Physical Biology of Flow. Princeton Univ Press, NJ
Van Dyke M (1982) An Album of Fluid Motion. Parabolic, Stanford
Ward-Smith AJ (1984) Biophysical Aerodynamics and the Natural Environment. Wiley, NY
Weis-Fogh T (1956) Biology and physics of locust flight. II. Flight performance of the desert locust (*Schistocerca gregaria*). Phil Trans R Soc Lond B 239: 459-510
Weis-Fogh T (1972) Energetics of hovering flight in hummingbirds and in Drosophila. J Exp Biol 56: 79–104
Weis-Fogh T (1973) Quick estimates of flight fitness in hovering animals, including novel mechanisms for lift production. J Exp Biol 59: 169–230
Weis-Fogh T, Alexander R McN (1977) The sustained power output from striaited muscle. In: Pedley TJ (ed) Scale effects in animal locomotion. Academic Press, London, pp 511–525
Weis-Fogh T, Jensen M (1956) Biology and physics of locust flight. I. Basic principles in insect flight. A critical review. Phil Trans R Soc Lond B 239: 415–458
Wilson JA (1975) Sweeping flight and soaring by albatrosses. Nature (Lond) 257: 307–308
Withers PC (1981) An aerodynamic analysis of bird wings as fixed aerofoils. J Exp Biol 90: 143–162
Wood CJ (1973) The flight of albatrosses (a computer simulation). Ibis 115: 244–256
Yates GT (1986) Optimum pitching axes in flapping wing propulsion. J Theor Biol 120: 255-276